ORGANIC BIOMARKERS IN ACTIVE AND FOSSIL TRAVERTINE DEPOSITS: LINKING THE PRESENT WITH THE PAST

by

JULIE FISER

(Under the Direction of Christopher Romanek)

ABSTRACT

Clues regarding the past history of microbial life on Earth may be deciphered from carbonate rocks given knowledge of the preservation potential of "biosignatures". Toward this end, active and fossilized microbial mats from Jackson Mountain travertine ridge (Nevada) were analyzed for grain fabrics, mineralogy, stable isotope compositions, and organic biomarkers within the context of a facies model to better understand preservation in carbonate hot springs.

Three distinct facies were recognized for active springs: 1) vent, 2) proximal slope, and 3) distal slope. Facies had similar $\delta^{13}C$ values for bulk biomass indicative of a C_3 fixation pathway; however, microbial phospholipid fatty acid and hydrocarbon biomarkers varied in composition.

The dominant attributes of fossil deposits were similar to the active springs, however the abundance of biomarkers varied. This study demonstrates that numerous attributes of fossil hot springs can be used to identify specific environmental conditions and microbial communities present during travertine deposition.

INDEX WORDS: travertine, biosignature, biomarker preservation, Jackson Mountain Travertine Ridge, Nevada, facies model

ORGANIC BIOMARKERS IN ACTIVE AND FOSSIL TRAVERTINE DEPOSITS: LINKING THE PRESENT WITH THE PAST

by

JULIE FISER

B.S., The University of Arkansas, 2003

A Thesis Submitted to the Graduate Faculty of The University of Georgia in Partial Fulfillment of the Requirements for the Degree

MASTER OF SCIENCE

ATHENS, GEORGIA

2008

© 2008

Julie Fiser

All Rights Reserved

ORGANIC BIOMARKERS IN ACTIVE AND FOSSIL TRAVERTINE DEPOSITS: LINKING THE PRESENT WITH THE PAST

by

JULIE FISER

Major Professor: Christopher Romanek

Committee: Gary Mills
Paul Schroeder

Electronic Version Approved:

Maureen Grasso
Dean of the Graduate School
The University of Georgia
May 2008

ACKNOWLEDGEMENTS

First and foremost, I would like to thank my advisor, Chris Romanek for taking a chance and responding to my initial inquiry. There are countless things that you have done that deserve recognition, but it is for the opportunity that I am the most grateful. I would also especially like to thank Gary Mills who always went above and beyond and who always knew what to say to motivate me. To Paul Schroeder and Chuanlun Zhang I would like to express my gratitude for always being available and providing insight into my project, as well as Heather Brant, Elizabeth Burgess, and Noelle Garvin who took a special interest in my project. It is hard to think of something they did not do, so thank you for everything. I would like to thank Suzette Walling for her guidance and experience in the field, and I would also like to thank Linda Jahnke and Roger Summons for taking time to provide samples and standards to ensure my hopanoid methods were accurate. Lastly I would like to thank my husband for always being supportive and providing encouragement when I needed it. This project was funded by NSF MCB-0348180 and the UGA cooperative agreement with the Department of Energy.

TABLE OF CONTENTS

LIST OF TABLES

Page

LIST OF FIGURES

Page

CHAPTER 1

INTRODUCTION

Keys to understanding the existence of life on early earth and potentially other planets are contained in the geologic record, but moreover, understanding the fossil record requires knowledge of the processes that lead to the preservation of biological markers in modern environments. Modern environments on Earth are dominated by prokaryotic microorganisms (bacteria and archaea) that are capable of existing anywhere there is liquid water, available carbon, nutrients, and an energy source. These microorganisms are composed of organic compounds that retain the chemical signature of life. Some of these compounds are biomarkers, which are organic compounds with complex structures indicative of specific organisms or communities that are chemically stable or degrade during sedimentation and diagenesis (Peters and Moldowan, 1993). There are four major classes of biomolecules that qualify as biomarkers: nucleic acids, proteins, carbohydrates, and lipids (Waggoner, 2002). Lipids are most widely used as biomarkers because they are structurally diverse and geologically stable (Boshecker and Middleburg, 2002).

Lipid Biomarkers

Membrane lipid biomarkers originate from lipid bilayer membranes in prokaryotic microorganisms. Membrane lipids, primarily phospholipids, are an amphiphilic molecule, which means they consist of a polar head and non-polar hydrocarbon tails(Fig. 1 a-b). Membrane lipids form a bilayer so that the hydrocarbon tails point inward and the polar heads are oriented towards the exterior of the membrane (Peters et al, 2005). This lipid bilayer membrane is essential for the

existence of all life and the structure of the membrane is varied among bacteria. Bacteria have typical lipid bilayer membranes composed of phospholipid fatty acids and isoprenoid hydrocarbons (see below), and some of these are diagnostic for specific taxa (Brocks and Summons, 2003).

Phospholipid Fatty Acids

Phospholipid fatty acids (PLFA) have the highest taxonomic specificity, and therefore are the most-well studied group of lipid biomarkers. Phospholipids consist of two hydrophobic hydrocarbon chains (non-polar tails) linked to a phosphorylated glycerol, typically referred to as the hydrophilic (polar) head (Peters et al, 2005). In high or low temperature environments, phospholipid membranes may become disordered or condensed, respectively. To maintain the integrity of the membrane, bacteria regulate the fatty acid length and number of double bonds (Peters et al, 2005).

Phospholipid fatty acids (PLFA) are analyzed in the form of fatty acid methyl esters (FAME). Fatty acid methyl esters are conventionally reported in the form of x:yωz. Where x is the number of carbon atoms in the non polar tail, y is the number of double bonds, and z is the location of the first double bond starting with the carbon atom furthest from the carbonyl carbon, referred to as ω. Double bonds can be in the cis or trans configuration; where carbon atoms are on the same side of the double bond for the cis configuration and opposite sides for trans configuration. Cyclopropane rings are also present in some fatty acid and are referred to as x:y cyc . Terminally branched fatty acid methyl esters are referred to as anteiso- and iso- fatty acids. Anteiso- fatty acids are branched at ω-3 position, and iso-fatty acids are branched at ω-2 position. Diagnostic groups of biomarkers can be specific to different classes of organisms. For example, iso- and anteiso- 15:0 to 17:0 are primarily associated with heterotrophic bacteria (Ray

et al., 1971) and Aquificales are commonly associated with the biomarkers 20:1ω9, 18:0, 18:1ω9, 18:1ω7 (Jahnke et al., 2001). Characteristic PLFA biomarkers for cyanobacteria and green non sulfur bacteria are 16:1ω7, 18:2ω6, and 18:1ω9c (Zhang et al., 2004).

Isoprenoid Hydrocarbons

Isoprenoid hydrocarbons are composed of a five carbon structure called isoprene (Fig. 2a). The typical linkage for isoprene units is "head to tail", however other linkages occur. "Head to tail" linkages produce acyclic isoprenoid hydrocarbons (Fig. 2b). Other linkages, such as "tail to tail" or "head to head" combinations form both acyclic and cyclic isoprenoids (Figs. 2c, 2d). Similar to PLFAs, isoprenoid hydrocarbons are incorporated into the lipid bilayer of microorganisms to maintain the integrity of the membrane (Peters et al., 2005). Isoprenoid hydrocarbons include biomarkers groups such as hopanoids (Peters et al., 2005). Hopanoids are ubiquitous and composed of the hopane molecule; however, different bacteria are known to produce specific bacteriohopanepolyols (Farrimond et al., 2000). For example 2-methyl bishomohopanol is diagnostic of cyanobacteria (Summons et al., 1996).

Preservation of Biomarkers

It is generally accepted that only one percent of organic carbon is preserved in sedimentary environments (Engel and Macko, 1993). This fact makes the long term preservation of biomarkers a low probability event; therefore understanding the degradation of biomarkers may give us a better understanding of the significance of the residual carbon present in the rock record. This may be accomplished by studying specific sites where the probability of biomarker preservation in modern environments is the greatest. These modern environments hold the key to understanding the relationships between living and fossilized microbial communities (Kidwell and Flessa, 1995).

Modern Environments

Fine-grained detrital systems and chemically mineralizing environments aid in preservation. Detrital systems are usually subject to compaction which contributes to preservation by: 1) incorporating organic molecules into clay structures such as interlayer sites, and 2) by promoting anoxia, which allows for mineralization and preservation of organic matter (Farmer and Des Marais, 1999).

Chemically mineralizing environments will permineralize microorganisms during early diagenesis (Farmer and Marias, 1999), and one such environment where this commonly occurs is travertine hot springs. In the nomenclature proposed by Ford and Pedley (1996), travertine refers to nonmarine calcium carbonate deposits that form from high temperature systems, (50-100°C), whereas tufa refers to precipitates at or below 50°C. Carbonate precipitation in hot spring environments produces layered deposits that may preserve a record of microbial activity at the point in time when each layer was deposited (Fouke et al., 2000; Atabay 2002). For the purposes of this study, active travertine deposits are defined as sites where the precipitation of $CaCO_3$ is presently occurring at temperatures up to 100°C and inactive travertine deposits are low temperature locations where deposition is no longer occurring.

Travertine Deposits

Travertine depositing springs in the western U.S. have water temperatures ranging up to 100°C. Based on morphology, there are five different types of travertine deposits: 1) waterfall or cascade deposits; 2) lake-fill deposits; 3) steeply sloping mounds, fans, or cones; 4) terraced mounds; and 5) fissure ridges (Chafetz and Folk, 1984). Waterfall travertine systems vary widely and typically encrust plants dominated by algae and mosses. Lake-fill deposits have horizontally stratified thin layers of carbonate that can continue laterally for many meters. Sloping mounds,

fans, and cones are accumulations similar to the lake fill deposits only they do not continue laterally, but strata are irregular and dipping. Terraced mounds derive their name from their step-like pattern, known as terraces. Finally, fissure ridges typically form in fault step over zones, and have a central fissure that occurs at the top of the ridge with steeply sloping sides (Pentecost, 2005). The steeply sloping sides typically have microterracettes, which are similar to the terraces of the terraced mounds but they are only a few centimeters in width (Chafetz and Folk, 1984). Exposed fossil deposits reveal laminated deposits that are parallel to the surface.

Facies Model

Travertine hot springs may be described using a facies model. According to Reading (1986), "A facies is a body of rock with specified characteristics." These characteristics are distinctive of specific conditions during sedimentation, which correlate to processes within that environment. In this study facies will be defined by systematic changes in morphological and geochemical characteristics of a body of sediment. Facies associated with travertine deposits vary depending on the geochemical and biological attributes of the depostitional system (Chafetz and Folk, 1984; Fouke et al., 2000; Atabey, 2002), and facies models correlate the geochemistry, petrography, and biology of these environments.

Fouke (2000), conducted a comprehensive analysis of the aqueous geochemistry, grain fabrics and mineralogy, and geochemistry of a hot spring (AT-1) at Mammoth Hot Springs in Yellowstone National Park and he used these parameters to partition the hot spring into different facies. Fouke analyzed the composition of the bacterial communities using bacterial 16S rRNA gene sequences and showed that communities inhabiting each facies were 87 % unique (Fouke et

al., 2003). Further investigations of bacterial communities by Zhang et al. (2004) demonstrated partitioning of PLFA biomarkers were consistent with the 16S rRNA findings and showed strong facies partitioning.

At Angel Terrace (AT), Fouke identified five facies: 1) vent, 2) apron and channel, 3) pond, 4) proximal slope, and 5) distal slope. The vent facies had the appearance of mounded travertine, with water temperature ranging between 69° and 72°C and a pH of 6.2 to 6.7. The carbonate deposits were composed of aragonite needles which formed fabrics consisting of hemispherical mounds that were 1 to 10 cm in width. Other studies have characterized lily-pad structures from the vent facies (Renaut and Jones, 2000), however these were not described at AT-1. These lily pad structures form in shallow waters, and are sub-aerially exposed. Bacterial sequences affiliated with *Aquificales*, a filamentous bacterium that forms long streamers, dominated the vent (Fouke et al., 2003). PLFAs were dominated by the fatty acids 20:1ω9, 18:0, 18:1ω9, and 18:1ω7, characteristic of Aquificales. Long carbonate tube encrustations that encased filaments of Aquificales were found throughout the aragonite fabric of this facies (Fouke et al, 2000).

The vent facies transitioned into the apron and channel facies at a temperature of 65° to 72°C and a pH of 6.5 to 7.0. These deposits were composed of primarily aragonite needle botryoids that formed mounded travertine. There was a higher diversity of bacteria in apron and channel facies as determined by bacterial sequences, however Aquificales dominated the bacterial community in this facies as well (Fouke et al., 2003; Zhang et al. 2004).

Fouke next identified the pond facies which consisted of large terraced pools. The pond facies had temperatures between 35° and 59°C and a pH of 7.4 to 8.6; they were composed of

both calcite and aragonite. Fabrics identified in the pond facies included shrubs, ice-sheets, and calcified bubbles. Fouke (2003) found the pond facies to have the highest diversity of bacterial species, although it was dominated by β-proteobacteria. Fatty acids that characterized the pond facies were 16:1ω7c, 18:2ω6, and 18:1ω9, which are consistent with cyanobacteria and green non sulfur bacteria (Zhang et al., 2004).

Fouke next identified the proximal slope facies which ranged in temperature from 38° to 5 in this facies (Fouke, 2000). 16s rRNA gene types contained a high diversity, dominated by α-proteobacteria, β-proteobacteria, and cyanobacteria. Lipid profiles were very similar between the pond and proximal slope facies at Angel Terrace and were dominated by cyanobacteria (Zhang et al. 2004).

The final facies Fouke identified was the distal slope facies, which had the lowest temperatures in the range of 18° to 38°C and a pH of 8.2 to 8.7. Blocky calcite and dendritic "feather" crystals formed shrub type fabrics in this facies. Bacterial 16s rRNA gene sequences were dominated by α-proteobacterial, β-proteobacteria, and cyanobacteria, similar to the proximal slope. Distal slope facies were characterized by an increase in the presence of 18:3 fatty acids which are associated with cyanobacteria, and i15:0 that is associated with heterotrophic bacteria (Zhang et al, 2004).

Interpreting Diagenesis

While facies can be attributed to specific environments, microbial mat communities have low preservation potential and carbonate rocks are easily susceptible to diagenetic alterations (Bathhurst, 1976; Farmer and Marais, 1999). Therefore, the ability to interpret these structures in ancient rocks requires knowledge of the transformations that occur after sedimentation (Theil et

al., 1997). Diagenesis can hamper interpretation of data, including mineralogy and grain fabrics, organic carbon and nitrogen composition, and lipid biomarkers.

The two major changes occurring during early diagenesis of travertines are cementation of porous sediments and the transformation of aragonite to low magnesian calcite (Pentecost, 2005). These changes also affect the $\delta^{18}O$ value of carbonates. Recrystallization can change the $\delta^{18}O$ value of the carbonate, sometimes reflecting conditions under which diagenesis occurred.

Early diagenetic alterations have also been shown to affect the concentration and isotopic composition of organic nitrogen and carbon in sediments and rocks (Freudenthal, et al, 2001). Microbial activity has been shown to cause both an increase and decrease in the $\delta^{13}C$ and $\delta^{15}N$ value of organics, however aerobic degradation by heterotrophic bacteria typically causes a decrease in organic nitrogen and carbon and increase in remaining $\delta^{13}C$ and $\delta^{15}N$ values (Freudenthal et al., 2001). Enrichment of $\delta^{13}C$ and $\delta^{15}N$ values occur over time due to discrimination of microbial reactions against the heavier isotopes (Nadelhoffer and Fry, 1994).

Diagenetic changes, such as defunctionalization of biomarkers can obscure lipid biomarker profiles. Phospholipid fatty acids are rapidly degraded upon the death of a microorganism, making this lipid group only applicable to extant microbial communities. Degradation of PLFAs yields n-alkanes and alkyl cyclohexanes (Brocks and Summons, 2003), among other compounds. Such degradation could confound interpretations, because n-alkanes are documented as primary constituents in some bacteria (Brocks and Summons, 2003).

While PLFA biomarkers are unstable, isoprenoid hydrocarbon biomarkers are geologically stable and have been found in rocks from the Archean (Boscheker and Middelburg, 2002; Brocks and Summons, 2003). Degradation of isoprenoid hydrocarbons produces structures

that are geologically stable. For example, hopanes are derived from bacteriohopanepolyols (Fig. 2c). During a series of reactions that occurs during diagenesis, the polyfunctionalized side chain is lost, converting bacteriohopanepolyol to hopane (Fig. 2d).

Therefore, clues regarding the past history of microbial life on Earth may be deciphered from carbonate rocks and minerals given some knowledge of the preservation potential of "biosignatures". Toward this end, the purpose of this study is to examine active and fossilized microbial mats from Jackson Mountain travertine ridge (Nevada) for grain fabrics, mineralogy, stable isotope compositions, and organic biomarkers within the context of a facies model and to better understand their preservation potential in a carbonate hot spring.

CHAPTER 2

MATERIALS AND METHODS

Study Site: Jackson Mountain Travertine Ridge, Nevada

Jackson Mountain Hot Spring is a travertine fissure ridge located on the southeastern edge of the Black Rock Desert in Nevada (Fig. 3). The ridge is positioned east to west with an active hot spring located at the western edge of the ridge (Fig. 4). The total length of the ridge is ~153m and it is subdivided into five sections (Fig. 5) based on morphology according to Pentecost (2005). Section 1, which is 34 m in length and of mound-type morphology, contains an active hot spring and recently active deposits, while Sections 2 through 5 are inactive. Section 2 is east of Section 1, 59 m in length, and relatively flat. Layered deposits are exposed in one portion of this section. Section 3 is ~28 m long, relatively flat, and it does not contain any recognizable facies or layers. Section 4, located on the east side of the ridge, is 15 m long, and contains a large structure of positive relief, known as a regular-type fissure ridge that has partially degraded to expose multiple layers of travertine. Section 4 has two dominant fabrics: 1) an exterior lamination that is porous and dark gray in color, and 2) interior microterracette laminations with an orange pigmentation. Section 5 is the western most portion of the ridge; it is ~15.8 m in length, and highly eroded.

Sample Collection

The locations of active hot spring samples were selected based on facies identification considering temperature, pH, distance from the vent, and observable microbial mats. Samples of

living microbial mat (Section 1) collected for lipid analysis were placed in sterile containers and stored on dry ice. Once samples arrived at the laboratory (~7 days), they were stored at -80°C until extraction.

Rock samples were collected over differing spatial and temporal scales for two inactive sections of the travertine ridge (Section 2 and 4). Cores of the ridge were taken using a Modified Tanaka 262 Engine Drill at Section 2 where layers were readily identified. Hand samples of these layers were collected as well to obtain material that had experienced subaerial exposure. Core samples were split lengthwise and one half was used for mineralogical and petrographic analysis and the other for lipid extraction.

Water Chemistry

Water temperature and pH were determined using a Corning 313 pH and temperature probe. Calibration of pH probe was performed at ambient temperature (~25˚C). Test kits by Hach were used for the following analysis in the field: SO_4^{2-}, S^{2-}, NO_2^- , NO_3^-, NH_4^+, Fe^{total}, Fe^{2+}, SiO_2, and PO_4^{3-}.

X-Ray Diffraction

The mineralogy of all samples was determined by X-Ray powder diffraction (XRD). Samples were ground using a Fritsch Planetary Mill at 300 rpm for 2 minutes to achieve a particle size of approximately 20 microns. The bulk mineralogy of powdered samples was determined using an X2 advanced Scintag diffraction system, using $CuK\alpha_1$ radiation (45.0 V, 40.0 mA) over the range 10 to 80˚ 2θ. Scan rates were conducted using a step scan mode with a step size of 0.02˚ count times per step, while calcite and aragonite peak areas were determined using a scan over the range of 25 to 30˚ 2θ, and a step size of 0.005˚. Background was not removed prior to peak integration. Calcite was identified by a sharp peak at 3.03Å, while

aragonite was identified using two diagnostic peaks centered at 3.53 Å and 3.46 Å. A calibration curve was obtained by mixing pure calcite and aragonite in different ratios, and measuring the $I_c/(I_c+I_a)$ ratio where I_c is the peak area of calcite and I_a is the peak area of aragonite (Davies and Hooper, 1963). Using this ratio, the theoretical wt % calcite was calculated using the non-linear regression,

$$y=(6399.0863)/(1+EXP(-((x+1)-2.1038)/0.2644))$$

where y=theoretical wt % of calcite and $x=(I_c/(I_c+I_a))$. Theoretical wt % calcite was plotted against actual weight percent calcite to check accuracy (Appendix A). Samples were reproducible to better than ± 8.6 %.

Stable Isotopes

Bulk and carbon and oxygen isotope analysis was performed on carbonate samples according to the method of Carroll et al. (2006). Approximately 150 ug of powdered bulk sample were loaded into a 4 mL vacutainer™ and flushed with helium gas. Samples were acidified with 8 drops of concentrated phosphoric acid. After 24 hours, the samples were analyzed by Continuous Flow-Isotope Ratio Mass Spectrometry (CF-IRMS) on a GasBench II peripheral device to quantify $^{18}O/^{16}O$ and $^{13}C/^{12}C$ ratios of active and inactive samples. Stable isotope ratios were reported in per mil units (‰) using standard delta (δ) notation (Craig, 1957). Delta values were calibrated against the V-PDB international standard reference material using NBS 19, and were reproducible to better than ± 0.18 ‰ (1 standard deviation) for both $\delta^{18}O$ and $\delta^{13}C$.

Paleotemperatures were calculated using the paleotemperature equation of Craig (1965):

$$T(^{\circ}C)=16.9-4.2(\delta_c-\delta_w)+0.13(\delta_c-\delta_w)2$$

where T= temperature, $\delta_c=\delta^{18}O$ value of carbonate relative to PDB, and $\delta_w=\delta^{18}O$ value of water relative to PDB, which was calculated using:

$$\delta_w(PDB) = \delta^{18}O_{w(SMOW)} - 0.2$$

where $\delta^{18}O_{w(smow)}$ was an average of samples taken in 2004 (Appendix E). $\delta^{18}O_{w(smow)}$ values of samples collected in 2006 were on average 2 ‰ higher than 2004 samples. This translates to a 10˚C difference in paleotemperatures; therefore all paleotemperatures will be reported as ±10˚C.

Total organic carbon and nitrogen analysis of bulk powdered travertine was subjected to fuming acid digestion by wetting a sample of known mass and placing it in a desiccator over a bed of 12M HCl, until a pH of 2 was reached. Samples were then filtered using a .45µm polycarbonate membrane and rinsed with excess water to remove dissolved constituents (e.g. Ca and Cl) and allowed to dry. Once dried, elemental analysis-isotope ratio mass spectrometry was employed to measure the total nitrogen and carbon content and quantify $^{15}N/^{14}N$ and $^{13}C/^{12}C$ ratios of active and inactive samples using the micro-dumas technique. Approximately 2 to 60 mg of acid extracted sample were placed in individual pre-cleaned tin capsules and weighed to ± 1.0 µg using an ultramicrobalance. Capsules were then sealed and placed in the auto sampler of a Carlo Erba Elemental Analyzer attached to a continuous flow isotope ratio mass spectrometer [Finnigan Delta Plus XL (Finnigan-MAT, San Jose, CA)]. Samples were combusted to N_2 and CO_2 in oxidation-reduction furnaces, separated by gas chromatography, and then measured for $^{15}N/^{14}N$ and $^{13}C/^{12}C$ ratios on the mass spectrometer. A N_2 (g) working standard was admitted prior to each sample combustion for calibration to an international AIR standard (Mariotti, 1983). Stable isotope ratios were reported in per mil units (‰) using standard delta (δ) notation (Craig, 1957). External working standards of dogfish muscle and acetanilide were analyzed to determine external precision; these standards were reproducible to better than ± 0.11‰ (1 standard deviation) for both $\delta^{15}N$ and $\delta^{13}C$ values over .5 volts. Lower voltage below 0.5 volts for $\delta^{15}N$ were outside the range of acceptable linearity for accurate and precise measurments.

Carbon to nitrogen ratios were calculated using the % carbon and % nitrogen values determined from each sample.

Lipid Extraction

Lipid analyses were similar for active mat samples and inactive rock, although the amount of sample required and the protocols for lipid extraction differed. Prior to extraction, active mat samples were freeze dried and ground with a mortar and pestle. Approximately 5g of active mat sample was added to a 25mL centrifuge tube. Inactive rock samples required the removal of exterior contamination, which was accomplished by abrading the exterior with a steel brush. These samples were then ground using a planetary mill to approximately 20 µm in diameter (as described above). Approximately, 30 g of powdered rock was necessary to obtain sufficient lipid for quantification. Due to the relatively larger amount of this material being extracted, powdered rock samples were extracted in 200 mL teflon bottles instead of 25 mL centrifuge tubes and all the extraction solvents were doubled in volume. Given that a large quantity of sample was required, the powdered rock samples were placed on a shaker for the extraction.

Section 1 samples (active and recently active sites) were analyzed for both PLFA and hydrocarbon fractions, while inactive sections were only analyzed for hydrocarbons. Preliminary analyses of inactive hand samples found no PLFA, and were therefore not analyzed in inactive samples. Prior to extraction, internal standards 5α-androstane, 5α-cholestenol, and 1,2 dinonadecanoyl-sn-glycero-3-phosphocholine (PL, 19:0) were added to each sample for the hydrocarbon, sterol, and PLFA fractions to be fully characterized, respectively. For each extraction set, a blank sample was included to monitor for potential contamination.

The extraction, separation, and derivitization procedures are outlined in Fig 6. Lipids were extracted for 12 hours with a chloroform-methanol-50mM PO_4 buffer solution in the ratio of 1:2:0.8 (White et al., 1979). Following extraction, 5mL of nanopure water was added, the sample was then vortexed, sonicated, and allowed to sit for 12 hours. During this time, an upper aqueous phase separated from a lower organic phase. The sample was then centrifuged at 2000 rpm for 15 minutes. The organic phase was collected and dried under nitrogen. The lipid components were separated using silicic acid column chromatography (Zhang et al., 2004), which separates the neutral and polar lipid fractions. One half of the polar fraction was reserved for the analysis of archaeal lipids as part of another study. The remaining polar fraction was subjected to a mild alkaline hydrolysis to convert the fatty acids to fatty acid methyl esters (FAME) for analysis by gas chromatography; the neutral fraction was saponified and fractionated by silicic acid column chromatography into hydrocarbon and sterol/alcohol fractions. The sterol/alcohol fraction was reserved, and was not analyzed in this study, while the hydrocarbon fraction was analyzed by gas chromatography.

FAME and hydrocarbons were analyzed using both GC-FID and GC-MSD. A Hewlett Packard 6890 gas chromatograph (GC) was equipped with a flame ionization detector (FID) and a DB-5 column (30 m; .25 mm id), and an Agilent 5890 series GC was interfaced to an Agilent 5973 mass selective detector (MSD) fitted with a 30 m x 0.25 mm i.d. DB-5MS column. For both instruments, helium (13.0 p.s.i.), was used as the carrier gas, and the inlet temperature was maintained 250˚C. The temperature program for FAME analysis was as follows; 80˚C for 1 min, 10˚C/min to 150˚C, 2˚C/min to 190˚C, 3˚C/min to 235˚C, and finally 10˚C/min to 280˚C held for 20 min. Hydrocarbons were analyzed with a modified temperature program of 80˚C for 2 min

and 12˚C/min to 300˚C followed by 5˚C/min to 325˚C held for 2 min. The identification of both fractions was based on comparisons of GC-FID retention times and mass spectra with those of reference compounds.

Bacteriohopanepolyol Analysis

Bacteriohopanepolyols required a different extraction procedure from the PLFA and hydrocarbons. Freeze-dried samples from the active hot spring were added to 25 mL centrifuge tubes. Cholestenol was added as an internal standard to each sample for quantification, and a blank was analyzed with each set to account for contamination. Samples were then extracted with 15 mL of chloroform: methanol (2:1) on a shaker for 12 hours. After extraction, the samples were centrifuged at 2000 rpm for 15 min, and the supernatant was collected and dried under nitrogen.

The extract was treated with periodic acid and sodium borohydride to convert bacteriohopanepolyols to terminal alcohols according to Innes (1997). After complete drying, 3 mL of a tetrahydrofuran: water (8:1) mixture and 300 mg of periodic acid were added and the solution was stirred for 1 hr. Water (10 mL) was then added to each sample and the solution was vortexed for 30 sec. The samples were then extracted three times using 15 mL of hexane. The extract was dried under nitrogen, after which 3 mL of an ethanol: sodium borohydride mixture (3 mL: 100mg) was added and stirred. After 1 hour, 15 mL of 100mM potassium dihydrogen phosphate was slowly added. The samples were then extracted again with 15 mL of hexane three times and the extract dried under nitrogen

The hopanols produced by this procedure were then acetylated. Samples were derivatized by adding 4 mL of a 1:1 mixture of periodic acid: acetic anhydride. The mixture was heated at 50˚C for 1 h, and then allowed to sit overnight at room temperature. Samples were then dried under nitrogen.

The methods were tested using underivatized samples and derivatized samples containing a known mixture of hopanoids provided by Linda Jahnke (NASA AMES Research Center) and Roger Summons (Massachusetts Institute of Technology), respectively. The presence of hopanoids confirmed the methods described above were effective in the extraction and derivitization of bacteriohopanepolyols.

Hopanoids were analyzed using the GC-FID and GC-MSD with a temperature program of 180˚C for 1 min and 10˚C/min to 300˚C then 2˚C/min to 320˚C held for 25 min. The identification of hopanoids was based on comparisons of GC-FID retention times and mass spectra with those of reference compounds. Quantification was carried out by adding an internal standard of known concentration (cholestenol: 50ppm).

CHAPTER 3

RESULTS

The sample description, mineralogy, stable isotopes, and biomarkers analyses of the travertine ridge were assessed for each of the three sampled sections: 1) Section 1 consisting of active and recently active hot springs emanating from a travertine mound, 2) Section 2 consisting of a regular type layered deposits of travertine, and 3) Section 4 consisting of regular type travertine morphology with layered deposits consisting of two morphologies. Stable isotope analysis included: carbon, nitrogen, and oxygen isotope analysis of bulk and processed samples. Biomarker analysis included PLFA, bacteriohopanoids, and hydrocarbons, however PLFA and bacteriohopanoid biomarker analysis were only performed on selected samples from Section 1.

Sample Description

In the field sample collections for the active hot springs were based on facies boundaries defined by systematic changes in morphology and aqueous geochemistry; however, sample collection for inactive samples was based only morphological attributes.

Section 1: Active Hot Spring and Recently Active Sediment

Section 1 consisted of the active hot spring (Fig. 7a) and recently active deposits (Fig. 7b). The active hot spring contained three morphologically distinct facies (based on Fouke's terminology) which included: vent, proximal slope, distal slope. Springs emerged from vents at the top of Section 1, and converged down the south face of the mound along the western edge of the fissure ridge. When the site was visited in 2004 three vents were flowing (vent #1, #2, #3) while in 2006 only two of the three vents were active (vent #2, #3). Sampling locations and

geochemical data collected in 2004 are shown in appendices B thru E, while 2006 sampling locations are shown in Fig. 7a and geochemical data are summarized in Table 1 and appendix F.

The vent facies was identified by the emergence of spring water to the surface. Morphological attributes of the vent included red organic filaments called streamers (sample 1; Fig. 8a) and lily pad structures (sample 2; Fig. 8b).Vent 2 had red filamentous bacteria streamers growing directly below the vent while vent 3 had lily pad structures directly below the vent. Red streamers were able to be removed from their point of attachment to form sample # 1, while whole lily pad structures with their associated microbial mats were collected to form sample # 2. Therefore, sample # 2 contained a high percentage of carbonate, while sample # 1 was mostly organic. Recorded temperatures for vent facies for both years were between 54.3 and 74.4˚C, while pH measurements was consistently between 7.3 and 7.4.

The proximal slope facies was identified based on its immediate downstream location to the vent facies; the proximal slope facies contained microterracette structures (Fig. 8c-8e). In the active hot spring, spring water from all the vents converged down slope to form green microterracettes with attached white streamers. A surface sample composed of white streamers and green microterracettes composed sample # 3 (Fig. 8c), while a second sample that contained mostly green microterracettes comprised sample # 4 (Fig. 8d). Carbonate sediment containing little biomass was collected directly below the green microterracettes which (sample 5; Fig. 8e). The temperature at the microterracettes location was 60.8˚C with a pH of 6.2. Flow rate decreased relative to the vent outflow as spring water flowed over a broader area in a sheet like fashion.

The distal slope facies was identified directly downstream of the proximal slope; this facies was characterized by an absence of microterracettes. The sample collected from this facies

was a thick, organic mat that lacked any morphological structure (sample # 6; Fig. 8f). Little $CaCO_3$ was associated with this sample. This distal slope facies is a site of relatively low temperature (46.9˚C) and relatively high pH (8.6), and very low flow rates.

Just to the west of the active site samples was a small area where water was not flowing; however, it appears that it recently had been flowing because of the abundance of dried mat material (Fig. 7b). Morphological attributes of recently active samples collected in this area included: microterracettes and a "leathery mat" consisting of dried biomass. Microterracette morphologies were orange in color and were predominately $CaCO_3$ with little associated biomass (sample # 7; Fig. 9a). Directly below (~5 cm) this sample was a green organic layer followed by additional microterracettes containing little biomass (sample # 8; Fig. 9b). A white leathery mat was "draped" over recently active sediment (sample # 9; Fig 9c). This sample was easily peeled from the underlying sediment; it contained little $CaCO_3$. Directly below the white leathery mat was the sub-leathery mat (sample # 10; Fig. 9c). Similar to the mat above it, the sample was leathery in texture; however it was green in color. The sample was high in organic content, but had more sediment associated with it than the leather mat sample (#9).

Section 2: Inactive Hand and Core Samples

Section 2 was located east of Section 1, it is 59 m in length, and relatively flat (Fig. 10a). Outcroppings at Section 2 had no visible external morphological structures that could be seen to assign facies; however, microterracettes were observed in core samples, which is consistent with a proximal slope facies. Layered deposits were exposed in one portion of the section (Fig. 10a, b, c). These deposits were composed of thin (~1-2 cm) layers, that were grouped into six larger units: the uppermost layer (0-8 cm) was referred to as sample # 2A, followed by subsequent layers: # 2B (10-18cm), # 2C (28-41 cm), # 2D (50-61 cm), # 2E (91-99cm), and # 2F (109-119

cm). Hand samples were collected from each of these exposed layers. These deposits were porous and mostly dark to light gray in appearance, however in each sample there was some orange coloration. These samples are designated as the "hand samples" of Section 2. Thin sections were made at representative locations from layers C and D, both samples were dominated by porous course grained fabric and trace laminations (Fig. 11).

Cores were taken from some of the layers starting at the surface of layer C, to obtain unweathered samples for comparison with the hand samples. Cores 1 and 2 were approximately 53 cm in length, and core 3 was 61 cm in length (Fig. 12; 13). They were taken approximately 5 cm from each other, and approximately 20-30 cm from hand sample locations. The cores were split lengthwise, and divided into approximately 10 cm sections. The upper 10 cm of each core, referred to as Section A contained, for the most part, unweathered material equivalent (some weathering was observed at 1-3 cm) on a contiguous horizon to hand sample C below that, material between 20 and 35 cm, referred to as Section C, corresponds with layer D (Fig. 14).

Thin sections were made at representative locations from each core (Fig. 12 and 13) and cyclothemic banding consisting of three repeating fabric types were distinguished in the thin sections. The top 1 to 3 cm of each core consisted of weathered dark gray porous fabric that was course grained in thin section (Fig. 15). The remainder of the top 20 cm of each core was orange in color with the three alternating fabrics. They included: 1) corrugated bands, 2) thin micrite bands, and 3) thick carbonate bands. At approximately 20 cm, each of the cores transitioned from orange to gray in color (Fig. 12). Non-repeating fabric types found only in lower section of the core included: trace laminations and dendritic shrubs. Corrugated bands of lamination were dark orange in color (Fig. 16a; 16d) and had pore spaces immediately below that were filled with white cement (Fig. 16c; 16f). In thin section, the corrugated bands had a tubular and branching

fabric immediately above (Fig. 16b;16e). The second type of banding was composed fine grained, dark gray laminations referred to as thin micrite (Fig. 17:a-d). The thin micrite bands were dark gray in reflected light and contained inclusions (Fig. 17d). In contrast, the thick carbonate bands were wide and light colored in reflected light. Edges of the carbonate bands were flat and in thin section the carbonate was microcrystalline (Fig. 17:a-d). At approximately 23 cm the occurrence of microcrystalline calcite and trace laminations increased (Fig. 18a; 18b). Finally, dendritic shrubs were common in the lowermost portion of core 3 (Fig. 18c; 18d).

Section 4: hand samples

Section 4, located on the east side of the fissure ridge, was ~15 m long (Fig. 19 a-c). It contained a large structure of positive relief. This section contained two dominant fabrics: 1) an exterior lamination that was porous and dark gray in color (Fig. 20a), and 2) microterracette lamination with an orange pigmentation (Fig. 20b). Representative samples were collected from each morphology around the section. A portion of Section 4 was partially degraded to expose multiple layers of travertine comprised of the microterracette morphology (Fig 20c; 20d). Microterracettes were orange in color and approximately 1 to 2 cm in width. Representative samples were collected from each layer.

Thin sections were made for exterior lamination and microterracette morphologies from representative samples collected at Section 4. Exterior lamination samples were predominated by a porous, course grained fabric (Fig. 21a; 21b), however sample A4 was dominated by dendritic shrubs (Fig. 21c; 21d). Microterracette samples were dominated by dendritic shrubs and tubular branching fabrics (Fig 22; a-d).

Mineralogy

The mineralogy of rock samples was determined by XRD analysis and included most of the samples collected at Section 1, Section 2, and Section 4. The mineralogy of all samples was dominated by calcite and aragonite. Table 2 shows the weight % of calcite and aragonite for the samples that were analyzed. The mineralogy of each section is described below.

Section 1: Active Hot Spring and Inactive Sediment

The mineralogy of the active and recently active sites sampled at Section 1 were predominately aragonite. The lily pad structures (sample #2) located near vent 3 was 95 % aragonite. Likewise, samples from the proximal slope facies, as was the sub-green microterracettes (sample #5) from the proximal slope facies. In the recently active site, the dry microterracettes (sample #7) and sub-dry microterracettes (sample #8) had a similar composition of 98 % aragonite.

Section 2: Hand and Core Samples

The predominate mineralogy of the samples from Section 2 was calcite, although the hand samples consistently contained a higher wt % calcite than core samples. The hand samples were almost entirely calcite (>97 %) with the exception of the uppermost layer (2A), which was 74 % calcite. Alternatively, section A thru C of the cores were not consistent in wt % calcite with the exception of the lowest horizon, section D which was 97 % calcite. However, the sections A and C from each core were consistently lower in wt % calcite than their corresponding hand samples C and D.

Section 4: Hand Samples

The mineralogy of hand samples collected from Section 4 samples varied based on whether the sample was an exterior lamination or microterracette morphology. Samples that

were exterior laminations were predominately calcite (97 %), except for one sample (#4) that had a lower percentage of calcite (45 %). The microterracette samples largely consisted of aragonite (avg 95 ± 1 %, n=3). Samples for the exposed layers (C1-C5) were also consistent with the microterracettes of the hand samples and were dominated by aragonite (avg 91 % ±2, n=3).

Stable Isotopes

Bulk Carbon and Oxygen

The carbon and oxygen stable isotope composition of bulk powdered samples were analyzed from active and inactive samples (Fig. 23; Appendix G). The $\delta^{13}C$ values ranged from -2.0 to 0.5 ‰ and the $\delta^{18}O$ values ranged from -21.7 to -11.7 ‰. Among the samples, the active and recently active sites of Section 1 displayed the lowest values. In Section 1, the lily pad sample (sample # 2) had the lowest $\delta^{13}C$ (-2.0 ‰) and $\delta^{18}O$ (-21.4 ‰) values and the white streamers had the highest $\delta^{13}C$ (-0.3 ‰) and $\delta^{18}O$ (-16.5 ‰) values. Alternatively, the hand samples of Section 2 exhibited the highest values with $\delta^{13}C$ values ranging from -0.4 to 0.2 ‰ and $\delta^{18}O$ values ranging from -14.6 to -11.7 ‰. It is interesting to note that the core samples, which were collected in close proximity (inches) to the hand samples, were significantly lower in carbon and oxygen isotope composition with $\delta^{13}C$ values that ranged from -1.8 to 0.5 ‰ and $\delta^{18}O$ values that ranged from -21.7 to -15.1 ‰. In addition, sections between cores varied however there was a general trend towards lower $\delta^{18}O$ values in the core samples with depth in core 2. The exterior laminations at Section 4 had a similar range of $\delta^{13}C$ values (-1.0 to -0.7 ‰), however the $\delta^{18}O$ values for all samples except A4 were significantly higher (-15.5 to -13.1 ‰). Sample A4, was more similar to the microterracette samples with a $\delta^{18}O$ value of -18.8. Samples from the microterracettes of Section 4 had $\delta^{18}O$ values ranging from -20.6 to -17.5 ‰ and $\delta^{13}C$ values ranging from -1.2 to -0.77 ‰. Exposed layers were similar in $\delta^{18}O$ value (-19.1 to -18.2

‰) and $\delta^{13}C$ (-1.2 to 0.-77 ‰) to microterracette samples, however no temporal trend was observed. Overall, there was a positive trend between the $\delta^{13}C$ and $\delta^{18}O$ values for all of the samples except the exterior lamination of Section 4.

Paleotemperatures were calculated for the active and recently samples according to the procedures outlined above (See Appendix G). A $\delta^{18}O$ value for water of -10.3 ‰ was used based on the average of 3 samples measured by Mills et al. 2004. In 2006, additional samples were measured which averaged -12.4 ‰ this 2 ‰ difference suggests calculated paleotemperatures may vary considerably (± 10˚C) given the uncertainty in the $\delta^{18}O$ value of water at the time of carbonate deposition. Paleotemperatures estimated for the active samples were compared to measured temperatures to estimate the utility of the technique. The lily pad sample collected near the vent had an actual temperature of 74.4˚C, while the paleotemperature was 78˚C. Spring water temperature at the proximal slope facies was ~60˚C (Table 1), while paleotemperature estimates ranged between 47˚ and 75˚C. These observations show that paleotemperatures are meaningful, however they may vary ± 10˚C.

Paleotemperatures calculated for hand samples from Section 2 ranged between 22˚ and 36˚C. Core samples ranged between 39 and 80˚C. The exterior lamination samples from Section 4 ranged from 29 to 41˚C, with the exception of sample A4 which was 61˚C. Microterracette samples were distinct from the exterior lamination samples. Paleotemperatures ranged from 57 to 62˚C, while the hand samples were similar to that of the microterracettes ranging from 52 to 72˚C.

Total Organic Carbon and Nitrogen

Selected samples were analyzed for their carbon and nitrogen stable isotope composition. The $\delta^{13}C$ values of all the samples ranged from -29.6 to -20.1 ‰ and the $\delta^{15}N$ values ranged

from -5.6 to 12.3 ‰ (Appendix H). Low voltages (≤ 0.5 V) for $\delta^{15}N$ values produced highly variable results (see methods), however were included for purposes of comparison. Among the samples, Section 1 exhibited the lowest $\delta^{13}C$ and $\delta^{15}N$ values (Figs. 24). The lily pad sample in Section 1 had the lowest $\delta^{13}C$ (-29.6 ‰) and $\delta^{15}N$ (-5.6 ‰) values.

Section 2 core samples had $\delta^{13}C$ and $\delta^{15}N$ values that were lower than the hand samples collected immediately adjacent to them. Core samples $\delta^{15}N$ values ranged from -2.6 to 2.8 ‰, and $\delta^{13}C$ values ranged from -26.3 to -25.8 ‰. Hand samples $\delta^{15}N$ values ranged from -0.4 to 6.0 ‰, and $\delta^{13}C$ values ranged from -21.7 to -26.7 ‰.

Samples from Section 4 varied more widely in their $\delta^{13}C$ and $\delta^{15}N$ values than samples from Section 2, however the exterior lamination samples had the highest $\delta^{13}C$ and $\delta^{15}N$ values of Section 4 samples. Exterior lamination samples were similar in $\delta^{13}C$ and $\delta^{15}N$ value compared to the hand samples collected from Section 2. Exposed layers of the proximal slope facies were distinct with $\delta^{13}C$ values ranging between -27.7 and -25.0 ‰ and $\delta^{15}N$ values ranging between -2.1 and 3.8 ‰.

C:N ratios were calculated using the % carbon and % nitrogen values in Appendix H. Ratios with N voltage < 0.5 V were rejected from further consideration. Section 1 samples in general had a C:N ratio of ~5 with the exception of the leathery mat and sub-leathery mat samples, while inactive samples varied ranging from 4.9 to 9.0. Section 2 hand samples had C:N ratios between 4.9 and 9.0. Section 4, exterior lamination samples ranged from 6.4 to 7.3, while the microterracettes ranged from 5.7 to 6.3. Exposed layers at Section 4 ranged from 6.8 to 10.8. There was no clear trend in the C:N ratio between sections or samples within a section.

Phospholipid Fatty Acids (PLFA)

Upon an organisms death the phosphorylated glycerol group of the phospholipid fatty acids (PLFA) is hydrolyzed and therefore, PLFAs represent only the extant microbial community. Preliminary experiments showed that PLFA only occurred in active sites samples of Jackson Mountain Travertine Ridge (JMTR), and therefore PLFA analysis was only conducted at Section 1. Samples that were analyzed included microbial biomass and sediment from the actively precipitating vents (active sites), and dried mat and sediment samples collected from recently active deposits (inactive sites).

Section 1: Active Hot Spring

Table 3 shows the distribution of PLFA (mol %) found in the active mat samples. Fatty acids ranged in carbon chain length from C13-C20 and include branched (iso and anteiso), unbranched, saturated, and unsaturated (ω) phospholipid fatty acids. Red streamers at vent 2 were separated from sediment during sample collection. Total PLFA biomass for the red streamers was the lowest of the active mat samples (36.0 µg/g). The lipid profile was dominated by 20:1ω (9c and 9t) and accounted for 40.9 % of the total fatty acid composition. The next most abundant fatty acids were iso and anteiso fatty acids 15:0 thru 17:0 (18.6 %), 18:0 (14.7 %), and unknown fatty acids (7.7%). Three isomers of 18:1ω (9c,7c,7t) combined to yield 6.6 % of the PLFA. Other fatty acids present were 20:2ω 6c (4.3 %) and 16:0 (4.2 %). Although 2-hydroxy 16:0 was only 3.0 % of the total FAME, it was highest in concentration in this sample compared to other samples from the active site. The lily pad structures contained a significant amount of microbial mat material, but they also included a substantial amount of carbonate. The total FAME concentration was relatively high (310 µg/g). The sample was dominated by 16:0 (30.0%), 18:0 (28.5%), and 18:1ω (7c, 7t, 9c, 5c) (14.0%). Furthermore, 18:1ω 9c and 5c

dominated the 18:1 isomers. This was markedly different from the red streamer sample, where 18:0 and 18:1ω (7c, 7t, 9c, and 5c) concentrations were approximately one half the concentration, and 16:0 was approximately a factor of seven lower. Other fatty acids in the lily pad sample included iso and anteiso 15 thru 17:0 (11.0 %), 20:2 (3.4 %), and unknowns (4.3 %). The fatty acids 20:1ω (9c and 9t) which were prevalent (40 %) in the red streamers sample only accounted for ~1.5 % of the total lipid composition. Finally the fatty acids 16:1ω (7c and 7t) were a very minor component of the lily pad sample (0.7 %), while they were not detected in the red streamer sample.

The active site samples collected from the proximal slope facies included white streamers, green microterracettes, and sub green microterracettes samples. The white streamer sample had relatively high FAME concentration (304 µg/g). The green microterracettes sample mat samples was predominately biomass, and accordingly had a high FAME concentration (439 µg/g). While the sub-green microterracettes sample was predominately carbonate, therefore total FAME concentration was relatively low (9 µg/g).

The white streamers sample was dominated by 16:0 (38.1 %), 18:0 (28.9 %), and 18:1ω (9c, 7c, 7t, and 5c) (16.1 %). Also 20:2 and unknown fatty acids decrease to 1.9 % and 2.1 %, respectively.

The green microterracettes sample was similar in lipid content to the white streamers sample. The most abundant fatty acids were: 16:0 (36 %), 18:0 (25 %), and 18:1ω (9c, 7c, 7t, and 5c) (18 %).

The lipid profile and total concentration of the sub-green microterracettes sample was markedly different from that of the green microterracettes sample immediately above it. Four points distinguish this sample from the green microterracettes sample: 1) the concentration of

FAME (8.6 µg/g), 2) the most abundant fatty acids were the iso and anteiso with carbon chains 15 thru 17:0 (22.6 %), 3) unknown fatty acids, 17:0, 15:0, and 17:0 cyc fatty acids were higher in abundance, and 4) 18:1 (9c, 7c, 7t, and 5c) were only composed of 18:1ω9 and were lower in abundance (4.0 %). Other abundant fatty acids were 16:0 and 18:0 with abundances 23.6 % and 10.0 %, respectively, although 18:0 was relatively low compared to the green microterracettes sample.

Among the proximal slope samples, fatty acid 18:0 concentration was highest in the white streamer sample. Also, generally there was an increase in 16:0 compared to the vent facies. The iso and anteiso fatty acids 15 thru 17:0 composed 7.7 %, a decrease from vent samples.

The orange mat sample was collected from the inferred distal slope facies; it had the highest total concentration of FAME (1146.1 µg/g) of all the active facies. This is understandable given this sample was collected as a thick microbial mat that contained little sediment. The dominant fatty acids were 16:0 (42.8 %), 18:1ω (9c, 7c, 7t, and 5c) (21.5 %), and 16:1ω (7c and 7t) (8.6 %). The concentration of each of these groups was the highest percent for all of the active site samples. Similar to the white streamers and green microterracettes samples, iso and anteiso fatty acids 15 thru 17:0 were 5.9 %. Unlike the other samples, the orange mat sample had the highest abundance of 18:2ω6c (4.1 %), a lower abundance of 18:0 (6.9 %), and a higher abundance of unknown (4.5 %). Of a particular interest, 20:1 ω (9c and 9t) concentrations were the lowest (0.3 %) of any active site samples.

Section 1: Recently Active Sites

Table 4 shows the concentration and distribution of lipids from sediment and mat material collected from the recently active site located adjacent to the actively flowing springs. The dry microterracettes sample contained a low total concentration of FAME (6.6 µg/g).

Dominant PLFAs were iso and anteiso 15 thru 17:0 (33.3 %), 18:1ω (9c and 7c) (19.9 %), 15:1ω4 (12.3 %), and 20:2 (9.2 %). Of particular interest, 15:1ω4 was not observed in any other active or recently active site sample and 20:2 had the highest concentration of any sample. Less abundant PLFAs included 16:0 (8.4%) and 16:1ω (7t) (6.5%). The concentration of 18:0 (2.8 %) was lower than all the active site samples. Unknown PLFAs accounted for 8.0% of this sample.

The sub-dry microterracettes sample contained very little PLFA (3.7µg/g). The most abundant PLFAs were iso and anteiso 15 thru 17:0 (36.2 %) with 16:0 being the second most abundant PLFA at 19.0 %, 20:2 at 12.7 %, and 18:0 at 9.8 %. The major differences in the dominant PLFAs between the sub-dry microterracettes and dry microterracettes sample were a lack of 15:1ω4, the presence of 17:0 cyc, and the increased percentage of 18:0 and 16:0, in the former sample. Both the dry terrace samples contained low mol percentages of 16:1ω7t and no 16:1ω7c.

The leathery mat sample had a total FAME concentration of 170.5 µg/g, which was the highest value for any of the recently active samples. This is not surprising given that this sample appeared to be composed of dried microbial mat. The most abundant PLFAs were 18:1ω (9c, 7c, 7t, and 5c) (34.3 %), 17:0 14-methyl (15.9 %), iso and anteiso 15 thru 17:0 (9.8 %), and 16:0 (17.2 %). Less abundant PLFAs were 16:1ω (7c and 7t) (12.5 %) and unknowns (8.0 %). In contrast to samples from the recently active proximal slope facies, 20:2 was not present.

The sub-leathery mat contained total FAME concentration of 84.8 µg/g, which was approximately one half that of the leathery mat above it. Little sediment was associated with this sample. Similar to the leathery mat, the most abundant fatty acid group was 18: 1ω (9c, 7c, 7t, and 5c) at 31.0 %.The next most abundant fatty acid group was 26:0 (21.6 %) followed by 16:1ω

(7c and 7t) at 11.0 %. The fatty acid 18:2ω6c was detected in significant quantities in this sample (6.5 %). Also present were 17:0 cyc (0.8 %), 19:0 cyc (2.2 %), 13:0 (1.2 %), and 14:0 (0.8 %). Similar to the leathery mat 20:2 was not present, however 14-methyl 17:0 decreased significantly. Unknown fatty acids comprised 4.9 % of the FAME.

Bacterial Hopanoids

As mentioned in the introduction, degradation of bacteriohopanepolyols will produce hopanes (which would be detected in the hydrocarbon fraction), therefore bacterial hopanoid analysis was only conducted at Section 1. Due to length of experiment representative samples from Section 1 were analyzed for bacterial hopanoids. Bishomohopanol and 2-methylbishomohopanol were detected in the sub-green microterracettes sample (#5) of the active site, the dry microterracettes sample (#7), and the leathery mat sample (#9) of the recently active site (Table 5). Concentrations were highest in the leathery mat sample.

Hydrocarbons

Hydrocarbon analysis was performed on all the samples collected from the Jackson Mountain travertine ridge, except the red streamers sample of the active site. Hydrocarbon total concentration and mol % abundance are reported below for each sample.

Section 1: Active Hot Spring

Hydrocarbon data for the active sites are reported in Tables 6. Samples from the vent facies included the red streamers and lily pad samples. The lily pad sample had a relatively low concentration of total hydrocarbons (9.0 µg/g), and only heptadecane (73.0 %) and 7-methyl heptadecane (27.0 %) were detected.

Samples from the proximal slope facies consisted of: 1) white streamers (#3), 2) green microterracettes (#4), and 3) sub-green microterracettes (#5). The concentration of total

hydrocarbons in the white streamers (28.9 µg/g) was higher than the lily pad sample. It was dominated by heptadecane (67.4 mol %) and 7-methyl heptadecane (7.6 mol %), although these values were lower than in the lily pad sample. Also present was phytane which represented 4.7 mol % of the total hydrocarbons, while unknowns accounted for 20.4 mol %. Just below the white streamers sample, the green microterracettes sample had a much lower concentration of total hydrocarbons (2.9 µg/g). Also, the sample had a lower abundance of heptadecane (48.6 mol %), while the abundance of 7-methyl heptadecane was relatively high at (27.1 mol %) and similar to the lily pad. No other known hydrocarbons were detected in this sample, and unknowns (24.4 mol %) were similar to the white streamers.

The sub-green microterracettes sample varied significantly from the other active site samples, although the total concentration of hydrocarbons was similar to the green microterracettes sample (2.6 µg/g). Many different hydrocarbons were detected such z-5-nonadecene (2.7 mol %), squalene (2.5 mol %), and 3-heptadecene (1.2 mol %). Heptadecane (3.1 mol %) and 7-methyl heptadecene (1.3 mol %) were significantly lower than in the other samples and phytane was detected at 1.8 mol %. Also interesting unknowns increased to 87.5 mol %.

The orange mat sample had the highest concentration of hydrocarbons (87.4 µg/g), but this is understandable given that this sample was composed almost entirely of microbial mat. Distribution of heptadecane (46.9 mol %), and 7-methyl heptadecane (18.1 mol %) were similar to the green microterracettes sample, however, 8-heptadecene and 3-heptadecene represented 4.0mol % and 3.7mol %, respectively, with the former hydrocarbon being distinct compared to all the other samples. Unknowns composed 27.3 mol % of the detected hydrocarbons.

Section 1: Recently Active

Hydrocarbon data for the recently active samples are reported in Table 7. Samples from the proximal slope facies had the lowest total concentration of hydrocarbons. The dry microterracettes sample had a significantly higher concentration (14.3 µg/g) than that of sub-dry microterracettes sample (0.7µg/g). The most abundant hydrocarbons in the dry microterracettes sample were heptadecane (42.9mol %) and 7-methyl heptadecane (6.6mol %). Also present were 8-heptadecene (1.7mol %), 3-heptadecene (2.0mol %), and z-5-nonadecene (0.8mol %). Phytane and squalene were detected, but very low in abundance. Unknown hydrocarbons totaled 44.5 mol %.

The sub-dry microterracettes had lower abundance of heptadecane (13.0 mol %). Squalene and phytane were present at a much higher percent abundance, 7.2 and 10.0 mol %, respectively. Unknowns were higher in the sub-dry microterracettes (69.8 mol %), than in the dry microterracettes.

The total concentration of hydrocarbons in the leathery mat sample was 50.3 µg/g. The leathery mat sample was dominated by heptadecane (56.3 mol %) and 3-heptadecene (15.6 mol %), followed by 8-heptadecene (7.2 mol %) and 7-methyl heptadecene (4.3 mol %). Unknowns composed 16.6 mol % of the total detected hydrocarbons.

The sub-leathery mat had a lower total concentration of hydrocarbons (41.7 µg/g) than the leathery mat sample. Similarly, the sub-leathery mat sample was also dominated by heptadecane (34.0 mol %) however, 7-methyl heptadecane was the next most abundant (31.9 mol %) followed by 3-heptadecene (17.7 mol %), and 8-heptadecene (4.2 mol %). 5 nonadecene was present in the sub-leathery mat (6.3 mol %), but not the leathery mat. Unknowns were the lowest in the sub-leathery mat (5.9 mol %).

Section 2: Inactive Hand and Core Samples

Table 8 shows the concentration and mol % of hydrocarbons from Section 2 at JMTR. Hand samples from Section 2 showed little variation in hydrocarbon content with the exception of the lowermost layer, which only contained squalene. The concentration of hydrocarbons in layers A thru D ranged from 0.7 to 1.2 µg/g, in layer F contained 0.1 µg/g. Sample E was lost during extraction procedures. The most abundant hydrocarbons were 7-methyl heptadecane (17.7 to 31.4 mol %) and heptadecane (8.4 to 14.1 mol %). 5-nonadecene was detected in samples A thru D (4.2 to 6.9 mol %), as well as squalene (4.7 to 7.9 mol %), while 3-heptadecene was present in samples A, B, and D (5.3 to 9.0 mol %). Samples B and D contained similar concentrations of 5-octadecene, 9-nonadecene, and eicosene, however these constituents were not observed in layer A, while 5-octadecene was absent from sample A and C. Layer F had a much lower concentration of hydrocarbons (0.1 µg/g) than the above layers, and squalene was the only hydrocarbon detected. Also, phytane was not detected in any of the samples

The concentration and distribution of hydrocarbons in the core samples that were collected adjacent to the hand samples are reported in Table 9. Core 1 had the highest concentration of total hydrocarbons in the top section A (1.6 µg/g) and in the bottom section D (1.0 µg/g), while sections C (0.3 µg/g) and D (0.6 µg/g) were lower. Heptadecane, 7-methyl heptadecane, 5 nonadecene, and eisosene were present in all sections, but they were highest in sections B and C, where total hydrocarbons were the lowest. Other hydrocarbons, such as squalene, phytane, and 3 heptadecane were only present in some layers. Squalene was present in all layers except D, and the concentration was highest in layer B (21.8 mol %). Layers A, B, and D contained small percentages of phytane (2.5 to 8.3 mol %). 3-heptadecene was only present in

sections A (2.0 mol %) and D (2.0 mol %). Unknown hydrocarbons ranged between 32 and 79 mol %.

Core 2 had the highest concentration of total hydrocarbons in section B (0.6 µg/g) and in the section C (0.4 µg/g), while sections A (0.3 µg/g) and D (0.3 µg/g) were lower. Heptadecane, 5 nonadecene, and 7-methyl heptadecane were present in all sections, except 7-methyl heptadecane was not detected in section A. Squalene was the most abundant hydrocarbon in sections A (19.3mol %), B (25.6mol %), and C (11.0mol %), while it accounted for only 4.3mol % in section D. Phytane was present in all layers except A, and eicosene was absent in all layers of core 2. Unknown hydrocarbons ranged between 60 and 74 mol %.

Total concentration of hydrocarbons was higher in every section of core 1, with the exception of section B. Section A of the cores had similar concentrations of heptadecane and 5-nonadecene, however core 2 did not contain any 7-methyl heptadecane and squalene was more abundant than core 1. Also it should be noted that lower abundance hydrocarbons detected in core 1 were not detected in core 2. Sections B and C of core 1 had higher concentrations of heptadecane, 7-methyl heptadecane, 5-nonadecene, and eicosene, while core 2 had a higher concentration of unknowns and squalene. Section D of the cores had similar concentrations of heptadecane, 7-methyl heptadecane, 5-nonadecane. Eicosene was only detected in core 1 and phytane and squalene were highest in core 2.

Section 4: Hand Samples

The total concentration and distribution of hydrocarbons from representative hand samples collected Section 4 were reported in Table 10. Sample of the exterior lamination from Section 4 showed variation in hydrocarbon content. The total concentration of hydrocarbons ranged from 0.7 to 1.8 µg/g. Hydrocarbons that were present in all four samples included;

heptadecane (8.8 to 21.5 mol %), and squalene (2.4 to 10.2 mol %). 7-methyl heptadecane was detected in all samples, except A1; and it was, however, the most abundant hydrocarbon in samples A3 (33.0 mol %) and A4 (25.9 mol %). Also present in samples A2, A3, and A4 was 3-heptadecene which ranged from 3.9 mol % to 16.2 mol %. Other hydrocarbons that were detected included 8-heptadecene, 1-heptadecene, 5-octadecene, 9-nonadecene, 5-nonadecene, eicosene, and phytane; however these biomarkers were not detected consistently. Unknowns varied widely between the samples and ranged from 9.9 to 67.7 mol %.

Representative hand samples of the microterracettes collected in Section 4 were variable in hydrocarbon biomarker abundances. Samples had total hydrocarbon concentrations ranging from 0.7 to 1.1 µg/g, respectively. 7-methyl heptadecane was the most abundant in samples B1 (29.7 mol %) and B2 (30.0 mol %), and heptadecane was the second most abundant at similar concentrations (13.7 and 17.6 mol %). Other hydrocarbons in samples B1 and B2 included: 3-heptadecene, 5-octadecene, 9-nonadecene, 5-nonadecene, and squalene. Also, 8-heptadecene and eicosene were detected only in sample B1, and unknowns varied between sample B1 (14.2 mol %) and B2 (25.0 mol %). Sample B3 was very different in hydrocarbon composition from the other microterracette samples. The most abundant hydrocarbons were 3-heptadecene (61.4 mol %) and heptadecane (27.0 mol %). There were no detectable unknowns, however, squalene, 5-nonadecene, and 5-octadecene were present in similar concentrations (~5 mol %).

There appears to be no distinct biomarker trends between the exterior lamination and microterracette samples. Variation in the presence of biomarkers, as well as mol % abundance was high between samples of the same morphological type.

Hand samples collected from the exposed layers in Section 4 had few hydrocarbon biomarkers (Table 11). The total concentration of hydrocarbons increased with depth at Section

4. The uppermost layer (C1) had 0.05 µg/g total hydrocarbons, while the lowermost layer (C5) had 0.37 µg/g. Sample C1 only contained squalene, while sample C2 contained heptadecane (59.1 mol %), 5-octadecene (22.6 mol %), and unknowns (18.3 mol %). Sample C3 contained heptadecane (38.2 mol %), squalene (16.9 mol %), and unknown hydrocarbons (44.9 mol %). The lowermost sample, C5 contained heptadecane (14.6 mol %), 5-octadecene (9.5 mol %), 5-nonadecene (22.9 mol %), squalene (9.0 mol %), and unknown hydrocarbons (44.0 mol %).

CHAPTER 4

DISCUSSION

Travertine hot springs provide a link to microbiological activity in the past by potentially preserving microbial biomarkers over spatial and temporal scales. Aqueous geochemistry, travertine morphology, geochemistry, and microbial biomarkers were characterized at the active facies in order to provide insights into fossil deposits at Jackson Mountain Travertine Ridge (JMTR) to better understand the preservation potential of lipid biomarkers.

Active Sites at Jackson Mountain Travertine Ridge

Jackson mountain hot spring consists of a series of environments that are divisible based on systematic changes in aqueous geochemistry, travertine morphology, mineralogy, and bacterial communities. Relative spatial position, temperature, and pH of the active hot spring were used to help define facies boundaries in the active sites. Measured temperatures were compared to independent estimates based on $\delta^{18}O$ values, so that temperature could be inferred from fossil deposits. Predominate bacterial groups were inferred from PLFA, hydrocarbons, BHPs, and organic carbon and nitrogen stable isotope analysis. As mentioned earlier, phospholipid fatty acid (PLFA) biomarkers are labile and were not expected in inactive samples; however hydrocarbon biomarkers are relatively stable geologically so they may provide a link between active and fossil travertine deposits. PLFA biomarkers were used primarily to relate the extant microbial community characteristics to hydrocarbon biomarkers in the fossil deposits. Stable carbon isotope compositions of organic matter provide further support to the interpretation of microbial communities by constraining potential carbon fixation pathways. For example,

cyanobacteria fix CO_2 via the Calvin cycle and typically have biomass $\delta^{13}C$ values range between -10 and -22 ‰ (Hayes, 2001). Aquificales fix carbon via the reverse tricarboxylic acid (rTCA) cycle, which result $\delta^{13}C$ values ranging from -4 to -13 ‰. Other carbon fixation pathways and their associated fractions are as follows: Acetyl-CoA (15-36 ‰), 3-Hydropropionate cycle (0 ‰), C4 and CAM (2-15 ‰) (Hayes, 2001). From these data collected at the active site three facies were distinguished and linked to organic geochemistry: 1) vent, 2) proximal slope, and 3) distal slope facies. Characteristics of each are described below. Mineralogy (aragonite) and $\delta^{13}C$ (-1.95 to -.030 ‰) values were consistent among active facies.

Vent Facies

Spring water emerging from the top of Section 1 marked the vent facies at JMTR. Vent facies at JMTR were characterized by relatively high temperatures, lily pad structures, relatively low stable isotope values for the carbon and oxygen isotope composition for bulk carbonates, and nitrogen and carbon stable isotope composition of organic matter. The two active vents in 2006 had similar temperatures (~73˚C) and pH (~7.4). Based on the $\delta^{18}O$ values for waters measured in 2004, calculated paleotemperatures agreed with measured temperatures, however when using 2006 $\delta^{18}O$ values the paleotemperatures are 10˚C lower than measured. Directly below the emerging spring water were red streamers surrounded by lily pad structures.

Vent facies were represented by two samples: red streamers and lily pads. Microbial communities of the red streamers and lily pads were distinct. PLFAs of the red streamers were dominated by 20:1ω9 (38 mol %) and a series of iso and anteiso branched fatty acids with carbon chains 15 thru 17 (18 mol %). The red streamers PLFA profile is consistent with the Aquificales bacterial group and heterotrophic bacteria. Aquificales are thermophilic chemolithotrophs that are commonly associated with filamentous streamers. Jahnke et al. (2001)

found that Aquificales cultures were dominated by 18:0, 20:1ω8n, and cyc 21:0. The PLFA structure of the red streamers sample is consistent with the findings by Jahnke for Aquificales, with the exception of cyc 21:0, which was not detected in this study. However, other studies of Aquificales biomarkers have concluded that 20:1ω8n, 18:0, and 18:1ω8n predominate and not cyc 21:0 (Kawasumi et al., 1984). Branched fatty acids (iso and anteiso) have not been reported for Aquificales cultures; therefore the series of iso and anteiso fatty acids 15 thru 17 in the red streamers sample (18 mol %) indicates an additional bacterial component. These branched fatty acids are common biomarkers for heterotrophic bacteria, such as genera *Thermus*, *Deinococcus*, and *Bacillus* (Wait et al. 1997).

While the lily pad sample was immediately adjacent to red streamer samples, it contained much less 20:1ω9 (1 mol %). The decrease in 20:1ω9 indicates the minor role of Aquificales in this sample. The detection of 16:1ω7t and 18:2ω6c, along with the increased abundance of 18:1ω (9c, 7c, 7t, 5c) are consistent with the presence of cyanobacteria or green non-sulfur bacteria (Ward et al, 1994; Summons et al, 1996). Hydrocarbon biomarkers provide further support for the abundance of cyanobacteria in the lily pad sample. Only two hydrocarbons were detected; heptadecane and 7-methyl heptadecane. 7-methyl heptadecane is particularly diagnostic for cyanobacteria (Dobson et al., 1988; Summons et al., 1996; Theil et al, 1997; Dembitsky et al., 2001). Finally, the carbon isotopic composition of the total biomass (-29.6 ‰) is also consistent with cyanobacteria (Hayes, 2001).

Proximal Slope Facies

Water cools after it leaves the vent and enters the zone referred to as the proximal slope facies. This facies is characterized by microterracette morphology, decreased temperatures, an increase in the stable carbon and oxygen isotope composition for bulk carbonate, and an increase

in the carbon and nitrogen stable isotope composition for organic matter. The measured temperature at the proximal slope was 61˚C, and the paleotemperature, calculated from 2004 $\delta^{18}O$ values of bulk carbonate ranged between 47 and 75 ±10˚C. Three samples were collected from this facies; 1) white streamers, 2) green microterracettes, and 3) the sub-green microterracettes.

The white streamers and green microterracettes samples had similar distributions of biomarkers. These samples displayed decreases in 20:1ω9 and iso and anteiso fatty acids 15 thru 17, which indicate a decrease in the abundance of Aquificales and heterotrophic bacteria, respectively, as compared to the vent red streamers sample. Also, PLFA biomarkers 16:1ω (7c and 7t), 18:2ω6c, and 18:1ω (9c, 7c, 7t, 5c) increased in green microterracettes, which suggests cyanobacteria and green non-sulfur bacteria increased in abundance (Ward et al., 1994; Summons et al., 1996). Hydrocarbons, 7-methyl heptadecane and heptadecane were also representative of cyanobacteria.

PLFA and hydrocarbon biomarkers were markedly different between the green microterracettes sample and the sub-green microterracettes sampled directly below. The total concentration of PLFA in the sub-sample was approximately 2 mol % of that in the surface layer, while the concentrations of hydrocarbons were similar. This is consistent with PLFA being degraded to produce hydrocarbons in the sub-surface. The changes observed in the PLFA profiles of the sub-green microterracettes also suggested an increase in heterotrophic bacteria biomarkers iso and anteiso 15 thru 17 biomarkers, and cyanobacterial biomarkers (18:1ω (9c, 7c, 7t, 5c)) decreased. The composition of hydrocarbon biomarkers were consistent with cyanobacteria in the sub-green microterracettes sample, however the sample exhibited changes including: 1) reduced percent abundance of heptadecane and 7-methyl heptadecane, 2) increased

percent of unknowns, 3) presence of phytane, squalene, 5-nonadecene, and 3-heptadecene, and 4) presence of 2-methylbishomohopanol and bishomohopanol.

The variations in biomarkers between the green microterracettes and sub-green microterracettes at JMTR support the conclusion that the surface sample is compositionally simple and the sub-surface sample increases in biomarker complexity. In a study by Dobson (1988), cyanobacterial mats were cored and hydrocarbon biomarkers were compared between an upper (0-3mm) and lower (12-15mm) horizon. Hydrocarbons seen in the upper mat were found in the lower mat, however additional hydrocarbons as well as different abundances were observed. Alkenes not observed in the top mat, for instance were observed in the lower mat. These variations in presence and abundance between the hydrocarbon fractions of the two horizons were attributed to 1) degradation or 2) input of new lipid biomarkers. The changes in PLFA biomarkers at JMTR represent a shift in microbial community structure to heterotrophic bacteria in the sub-green microterracettes. However it is difficult to elucidate whether variations observed in the hydrocarbon fraction at JMTR are the result of variation in the community or PLFA degradation. The similar total concentration of hydrocarbon biomarkers between the green microterracettes and sub-green microterracettes is surprising because associated biomass was higher in the green microterracettes sample. Perhaps if the percent carbonate was accounted for between the samples there would be an increase in the concentration of hydrocarbon biomarkers in the sub-green microterracettes. Geologically stable cyanobacteria biomarkers such as phytane, squalene, 2-methyl bishomohopanol, and bishomohopanol were all detected in the sub-green microterracettes, but not in the green microterracettes mat sample. Therefore, PLFA degradation

could account for the increase of unknown hydrocarbons, the reduced mol % abundance of 7-methyl heptadecane and heptadecane, and the presence of additional hydrocarbons in the sub-green microterracette sample.

Distal Slope Facies

A distal slope facies was recognized below and along the sides of the proximal slope facies. This facies was characterized by a lack of microterracettes and the presence of a thick orange microbial mat. The water temperature of the orange mat was 47˚C. Stable isotope analysis was not performed on the orange mat sample, due to limited quantity of sample.

Little carbonate was associated with the orange mat; therefore this sample had the highest concentration of PLFA (~1150 ppm) and hydrocarbons (~90 ppm). Cyanobacteria PLFA biomarkers (16:1ω (7c and 7t), 18:2ω6c, and 18:1ω (9c, 7c, 7t, 5c)) were the highest of all the samples collected in the active hot spring. Also 20:1ω9 abundance was the lowest for all samples, suggesting higher temperature groups such as *Aquificales* were absent from the lower temperature mat. Cyanobacteria hydrocarbon biomarkers, such as heptadecane and 7-methyl heptadecane, were also present and similar in abundances to the proximal slope facies. Interestingly, 8 and 3 heptadecene concentrations were the highest in the orange mat sample. This was the only active site where 8-heptadecene was detected. 8-heptadecene is known to be produced by cyanobacteria in small abundances (Dembitsky et al., 2001); it could be possible that it reached detectable concentrations in the distal slope facies.

Link between Active, Recently Active, and Inactive Sites

Jackson Mountain hot spring has facies that are distinguishable by travertine morphology, aqueous geochemistry, and lipid biomarkers; the knowledge gained from these relationships will be used to interpret recently active and inactive facies at JMTR. Using the active sites as a link to

other deposits at JMTR, petrography, mineralogy, and stable isotopes were combined to better understand the effects of diagenesis on the preservation of hydrocarbon biomarkers in travertine facies. The mineralogy of all three active site facies was aragonite.

Section 1: Recently Active Samples

The samples collected from the recently active site were inferred to be from a proximal slope facies based on their morphological structure (microterracettes), paleotemperatures, stable isotope composition, and lipid biomarkers. The four samples collected included: dry microterracettes, sub-dry microterracettes, leathery mat, and sub-leathery mat. The dry microterracettes and sub-dry microterracettes are predominately aragonite, suggesting that deposition was recent and at high temperatures. The leather mat (draped over sediment that was likely of the proximal slope facies) is predominantly dried biomass with little associated carbonate. Paleotemperatures calculated from the associated carbonate samples ranged between 62 and 75 ±10˚C, similar to the proximal slope facies in the active site. Furthermore the carbon isotope composition for the bulk samples were also similar to the proximal slope facies (-1.38 to -0.96 ‰).

Recently active dry microterracettes and sub-dry microterracettes samples are similar in PLFA composition to the green microterracettes and sub-green microterracettes in the active site, respectively. However, unlike the green microterracettes in the active site the dry terracettes are dominated by iso and anteiso fatty acids 15 thru 17, diagnostic of heterotrophic bacteria. Both recently active samples had a higher percent abundance of iso and anteiso fatty acids 15 thru 17 than in the sub green terracettes, which is most likely explained by the location being inactive and therefore dominated by heterotrophic bacteria. The cyanobacteria biomarkers 18:1ω (9c, 7c, 7t, 5c) and 16:1ω (7c and 7t) were also present in both samples. Total PLFA concentrations of

dry microterracettes and sub dry microterracettes samples were 1 % that of the active site. Furthermore, representative hydrocarbon biomarkers 7-methyl heptadecane, heptadecane, and bishomohopanol in the recently active samples were consistent with cyanobacteria and the active site proximal slope. The sub-green terracettes carbon isotope composition of the total biomass (-28.3 ‰) was similar to the proximal slope and cyanobacteria.

While the leathery mat and sub-leathery mat samples are similar in composition to each other and consistent with cyanobacteria, abundances are different than those seen in the proximal slope facies. The cyanobacteria biomarkers 18:1ω (9c, 7c, 7t, 5c) are more abundant than in the dry terracettes or green terracettes, however 16:1ω (7c and 7t) are also present but in lower concentrations. Heterotrophic bacterial biomarkers (iso and anteiso 15 thru 17) decreased compared the dry terracettes. Total PLFA concentrations for both samples were 40 % that of the active site proximal slope. Hydrocarbon biomarkers are distinct in the leather mat samples; bishomohopanol, 2-methyl bishomohopanol, and 3-heptadecene are the highest concentrations in the leathery mats. Finally, the carbon isotopic composition of the total biomass (-26.8 ‰) is also consistent with cyanobacteria (Hayes, 2001).

While recently active samples are consistent with proximal slope facies, there were temporal variations in the overlying and underlying samples of the recently active samples. Both PLFA and hydrocarbon fractions concentrations decreased in the “sub” samples, while percent abundance of unknowns for both fractions increased. This is likely explained by the degradation of phospholipids to hydrocarbons. Furthermore, the hydrocarbons squalene and phytane increased in abundance in the sub-dry microterracettes compared to the overlying dry microterracettes sample. Squalene is known to be produced in cyanobacteria, however it was observed in low concentration (Dembitsky et al., 2001). Since it is an isoprenoid hydrocarbon

and therefore geologically stable, the squalene likely increased in percent abundance relative to other compounds less resistant to degradation. Also, 7-methyl heptadecane increased in abundance in the sub-leathery mat sample compared to the leathery mat sample, which is consistent with its geological stability relative to other compounds such as heptadecane. However, this was not observed in the sub-dry microterracettes compared to the dry microterracettes. This could possibly be explained by the low total concentration of hydrocarbons in the sub-dry microterracettes sample.

Section 2: Hand and Core Samples

Cores were collected next to hand samples (Fig. 10) in Section 2, to evaluate the effect of subaerial exposure on the samples. Core fabrics, stable isotopes, and hydrocarbon biomarkers are similar to the proximal slope facies; however exposure to weathering appears to have significantly altered the hand samples. Overall data from the core samples is variable, which variation indicates changes that occur over small spatial scales. However, core data were consistently more similar to one another than to data from the hand samples.

Banding distinguished in the cores and thin sections are consistent with proximal slope facies, while hand samples lacked any morphologically distinct features. In particular, corrugated band laminations in the core thin sections were primary fabrics representative of microterracettes (Pentecost, 2005), while hand sample thin sections were course grained secondary fabrics.

Mineralogically, the core samples appear to be less altered than hand samples as indicated by the higher percent of aragonite. Section A of the cores ranged between 64 and 76 % calcite, where the corresponding hand sample (2C) was 97 %. Section C of the cores ranged

between 61 and 76 % calcite, where the corresponding hand sample (2D) was 97 %. The increased percent calcite in weathered samples is consistent with the transformation of aragonite to calcite in recrystallized fabrics.

Bulk carbon, oxygen, and nitrogen stable isotope compositions in core samples are similar to active and recently active proximal slope facies, however the corresponding hand samples have higher values. Calculated paleotemperatures for Section A of the cores averaged 42 ±10˚C, and the corresponding hand sample (2C) is 32 ±10˚C. Section C of the cores averages 54 ±10˚C, and the corresponding hand sample (2D) is 28±10˚C. The increased percentage of calcite and $\delta^{18}O$ values might indicate a lower temperature depositional environment, however it is unlikely given the proximity of sample collection.

Assuming the environments of deposition were similar between hand and core samples due to the physical proximity of the collection sites, it appears that exposure may also affect lipid geochemistry. The distributions of hydrocarbon biomarkers in the Sections A and C of the core samples were similar to those in the sub-green microterracettes and sub-dry microterracettes, while the distributions similar to those seen in the respective hand samples were not seen in active or recently active sites. Lastly, the ratio of heptadecane: 7-methyl heptadecane in the hand samples suggests degradation, because branched alkanes are more resistant to degradation than n-alkanes (Brocks and Summons, 2003). In all the active sites sampled and core samples, heptadecane was always more abundant that 7-methyl heptadecane, however in the hand samples the more geologically stable biomarker (7-methyl heptadecane) was more abundant.

Section 4: Representative and Exposed Samples

Travertine morphology, fabric, mineralogy, stable isotope composition, and the lipid biomarkers of representative samples of microterracettes and the exposed layers were all

consistent with proximal slope facies, while exterior lamination samples were dissimilar to facies seen in the active site. The two morphologies represented at Section 4 were microterracettes and the exterior lamination. The microterracette samples were orange in color with microterracette structures, while the exterior laminations were dark gray and porous and only existed on the outermost layer. Thin sections also varied between the two samples. Microterracette samples were composed of primary tubular branching and shrub fabrics; where as the exterior laminations were composed of a secondary course grained fabric. Microterracette samples were predominately aragonite with an average $\delta^{18}O$ value of -18.8 ± .5 , this is consistent with the proximal slope of the active site, and indicates either recent deposition or recent exposure with little alteration of original facies. Paleotemperatures were also consistent with proximal slope facies (61 ± 10˚C). Exterior lamination facies were predominately calcite with an average $\delta^{18}O$ value of -15.4 ±2.5 and an average paleotemperature of 41 ± 10 ˚C. Characteristics of the exterior lamination samples were not observed in the active site, and could be explained by low temperature deposition or degradation of original facies. However, both bulk and organic $\delta^{13}C$ values were higher than those seen in the active site facies, while the exterior lamination samples were higher than microterracette samples.

While the microterracette and exterior lamination samples were distinct in morphology, fabrics, mineralogy, and stable isotope composition there were no distinguishable trends in biomarker distributions. The exterior lamination and microterracette samples were collected from various locations so the broad hydrocarbon biomarker distributions observed could the due to spatial variation in microbial mats. Similar to the hand samples in Section 2, biomarkers were consistent with a proximal slope facies although 7-methyl heptadecane abundances were unlike

any observed in the active site samples. 7-methyl heptadecane a more geologically stable biomarker was more abundant than less geologically stable and typically more abundant hydrocarbon heptadecane.

Travertine morphology, fabric, mineralogy, stable isotope composition of the exposed layers of Section 4 were compatible with a proximal slope environment; however the biomarker distribution appears to be incompatible with this suggestion. The uppermost layer only contained squalene and none of the layers contained 7-methyl heptadecane. The total concentration of biomarkers was low, which could potentially explain why lesser abundant hydrocarbons were rarely detected.

Comparison of Geographically Isolated Active Travertine Hot Springs

Fouke's facies model was developed from spring AT-1 at Angel Terrace, Mammoth Hot Springs, Yellowstone National Park (Fouke et al, 2000). At Mammoth Hot Springs, the travertines form terrace and fissure ridge deposits. AT-1 is a terrace type travertine, whereas Jackson Mountain Travertine Ridge (JMTR) consists of both mound and ridge type deposits. A comparison of morphological features, water chemistry, mineralogy, and phospholipids fatty acids (PLFA) profile between Jackson Mountain Hot Spring and AT-1 show similarities which suggest the facies model of Fouke may be a more general characteristics of other travertine deposits.

Vent Facies

Vent facies were comparable between the two sites. Morphological similarities included a moulded appearance immediately at the vent with active filamentous "streamers" directly below. However, the pigmentation of the streamers varied between the two hot springs; at AT-1 they were white while at JMTR they were red. Temperature of the vent facies at JMTR was similar to

AT-1, while pH measurements were higher at JMTR. Aragonite was the dominate mineralogy between both hot springs. Phospholipid fatty acid profiles were consistent between the two hot springs. The most abundant fatty acids at the vent facies in both hot springs were 20:1w9c (AT-1: 26 %; JMTR: 38 %) and 18:0 (AT-1: 20%; JMTR: 15%). At AT-1, the next most abundant PLFA was 18:1, while at Jackson Mountain it was i17:0, indicating there was a higher percentage of heterotrophic bacteria present in JMTR. At both sites, 16:0 was a minor component (AT-1: 9 %; JMTR: 4 %). Overall both vent facies were markedly different from the other facies, and each site each was dominated by Aquificales and heterotrophic bacteria.

Proximal Slope Facies

The proximal slope facies at the two locations were similar and distinct from the vent facies. Microterracettes were the dominant morphology, although, proximal slope facies at JMTR contained green pigmentation versus the orange found at AT-1. Temperature ranges at AT-1 were between 38 and 55˚C, while the temperature at JMTR was 60˚C. The pH of the proximal slope facies varied at JMTR, and was higher at AT-1. Mineralogy at JMTR was aragonite; however, the mineralogy at AT-1 was a mix of calcite and aragonite. Lipid profiles for both hot springs displayed a decrease in 20:1w (9c and 9t) (AT-1: 0.1 %; JMTR: 1.0 %) and an increase in 16:0(AT-1: 58.7 %; JMTR: 32.6%) and 16:ω (7c and 7t) (AT-1: 5.9 %; JMTR: 1.3 %), which is indicative of the transition from Aquificales to cyanobacteria.

Distal Slope Facies

The distal slope facies (orange mat) at JMTR was morphologically indistinctive from other facies at this location. However, the temperature, pH, and lipid profiles differed from the proximal slope facies. The distal slope facies morphology at Jackson Mountain was different from the distal slope facies at AT-1. At JMTR, large terraces were not observed like those at AT-

1. However, pH and temperature, and lipid profiles were similar. There was a decrease in fatty acid 18:0 at JMTR and AT-1 to 7 % and 4 %, respectively, while 18:1ω (7c, 7t, 9c, 9t, 5c) remained unchanged compared to the proximal slope facies. Collectively the fatty acids 18:1 totaled 20 % and 25 % of the total PLFA at JMTR and AT-1, respectively. The most abundant fatty acid remained 16:0 in both hot springs. However, AT-1 showed a decrease in the total percent of 16:0, whereas JMTR the total % increased.

Therefore, based on this work it can be concluded that there maybe general characteristics for geographically isolated carbonate hot springs. These general characteristics can be used to link active and inactive travertine deposits, and better understand preservation of biomarkers.

CHAPTER 5

CONCLUSIONS

Facies at JMTR active sites are divisible based on a facies model using numerous attributes to identify specific environmental conditions. Using a facies model three facies were identified: vent, proximal slope, and distal slope. Each facies was composed of distinct aqueous geochemistry, travertine fabrics, and bacterial communities.

Vent facies had high temperature (74˚C), lily pad structures, and were dominated by Aquificales and heterotrophic bacteria. Few geologically stable hydrocarbons were associated with this facies, only 7-methyl heptadecane in the lily pad structures.

Proximal slope facies were marked by a decrease in temperature, microterracette structures, increased stable isotope compositions, and dominance of cyanobacteria. Geologically stable biomarkers for cyanobacteria associated with the proximal slope included: 7-methyl heptadecane and 2- methyl bishomohopanol.

Distal slope facies decreased in temperature from the proximal slope, they had few morphological attributes, and were dominated by cyanobacteria.

Multiple attributes were used to assign facies of inactive samples and better interpret biosignatures including: grain fabrics, mineralogy, stable isotope compositions, and organic biomarkers. Temporal variations existed in the recently active proximal slope, however it is difficult to elucidate whether changes were a result of changes in microbial community or

degradation of biomarkers. In addition cores indicated that exposure to weathering may affect all biosignatures and changes may occur over small spatial scales, which could lead to misinterpretation of facies.

A comparison of Jackson Mountain hot spring to Angel Terrace revealed that two geographically isolated travertine hot springs were overall consistent in facies and facies attributes.

REFERENCES

Atabey, E., 2002. The formation of fissure ridge type laminated travertine-tufa deposits microscopical characteristics and diagenesis, Kirsehir Central Anatolia. Mineral Res. Expl. Bul., 123-124: 59-65.

Boschker, H.T.S., Middelburg, J.J., 2002. Stable isotopes and biomarkers in microbial ecology. FEMS Microbial Ecology, 40: 85-95.

Brocks J. J. and Summons R. E., 2003. Sedimentary hydrocarbons, biomarkers for early life. In Treatise in Geochemistry, Vol. 8 (ed. H. D. Holland), 53pp. in press Elsevier.

Carroll, M., Romanek, C., and Paddock, L., 2006. The relationship between the hydrogen and oxygen isotopes of freshwater bivalve shells and their home streams. Chemical Geology, 234:211-222.

Chafetz, H.S., and Folk, R.L., 1984. Travertines: depositional morphology and the bacterially constructed constituents. Journal of Sed. Pet., 54(1): 0289-0316.

Craig, H., 1957. Isotopic standards for carbon and oxygen and correlation factors for mass-spectrometric analysis of carbon dioxide. Geochimica et Cosmochimica Acta, 12; 133-149.

Craig, H.,1965. The measurement of oxygen isotope paleotemperature. In: Tongiorgi, E. (Ed.), Stable isotopes in Oceanographic Studies and Paleotemperatures. Cons Naz delle Rich. Laboratorio di Geologia Nucleare, Pisa, 161-182.

Davies, T.T., and Hopper, P.R., 1962. The determination of the calcite: aragonite ratio in mollusc shells by X-ray diffraction. Mineralogical Magazine, 33 (262): 608-612.

Dembitsky, V.M., Dor, I., Shkrob, I., and Aki, M., 2001. Branched alkanes and other apolar compounds produced by the cyanobacterium *Microcoleus vaginatus* from the Negev Desert. Russian Journal of Bioorganic Chemistry, 27 (2); 110-119.

Dobson, G., Ward, D.M., Robinson, N., and Eglinton, G., 1988. Biogeochemistry of hot spring environments: extractable lipids of a cyanobacterial mat. Chemical Geology, 68; 155-179.

Engel, M.H., Macko, S.A., 1993. Organic geochemistry: Principles and applications. Plenum Publ. Corp., New York. 861 p.

Farmer, J.D., Marais, D.J., 1999. Exploring for a record of ancient life Martian life. Journal of Geophysical Research, 104(E11): 26,977-26,995.

Farrimond, P.; Head, I. M.; Innes, H. E., 2000. Environmental influence on the biohopanoid composition of recent sediments. Geochimica et Cosmochimica Acta, 64(17), 2985-2992.

Ford, T. D., and Pedley, H. M., 1996. A review of tufa and travertine deposits of the world. Earth-Science Reviews, 41(3-4); 117-175.

Fouke, B.W., Farmer, J.D., Des Marais, D.J., Pratt, L., Sturchio, N.C., Burns, P.C., and Discipulo, M.K., 2000. Depositional facies and aqueous-solid geochemistry of travertine-depositing hot springs (Angel terrace, Mammoth Hot Springs, Yellowstone National Park, U.S.A.). Journal of Sedimentary Research, 70(5):565-585.

Fouke B. W., Bonheyo G. T., Sanzenbacher B., and Frias-Lopez, J., 2003. Partitioning of bacterial communities between travertine depositional facies at Mammoth Hot Springs, Yellowstone National Park, U.S.A. Can. J. Earth. Sci., 40:1531-1548.

Freudenthal, T., Wagner, T., Wenzhofer, F., Zabel, M., and Wefer, G., 2001. Early diagenesis of organic matter from sediments of the eastern subtropical Atlantic: Evidence from stable nitrogen and carbon isotopes. Geochimica et Cosmochimica Acta, 65:11; 1795-1808.

Hayes, J.M., 2001. Fractionation of carbon and hydrogen isotopes in biosynthetic processes. Reviews in Mineralogy and Geochemistry Vol., 43; 225-278.

Innes, H., Bishop, A.N., Head, I.M., Farrimond, P., 1997. Preservation and diagenesis of hopanoids in recent lacustrine sediments of Priest Pot, England. Organic Geochemistry, 26; 483-488.

Jahnke, L.L., Eder, W., Huber, R., Hope, J.M., Hinrichs, K.U., Hayes, J.M., Des Marais, D.J., Cady, S.L., and Summons, R.E., 2001. Signature lipids and stable carbon isotope analyses of octopus spring hyperthermophilic communities compared with those of *Aquificales* representatives. Appl. Environ. Microbiol., 67: 5179-5189.

Kawasumi, T., Igarashi, Y., Kodama, T., and Minoda, Y., 1984. *Hydrogenobacter thermophilus* gen. nov., sp. Nov., an extremely thermophiliec aerobic, hydrogen-oxidizing bacterium. Int. J. System. Bacteriol., 34; 5-10.

Kidwell, S.M., Flessa, K.W., 1995. The quality of the fossil record: populations, species, and communities. Annu. Rev. Ecol. Syst., 26:269-299.

Mariotti, A. 1983. Atmospheric nitrogen is a reliable standard for natural ^{15}N abundance measurements. Nature, 685-687.

Mills, G., Li, Y., Jones, M., Paddock, L., Romanek, C., Zhang, C., and Wiegel, J., 2004. Chemical and isotopic signature of hot springs at Jackson Mountain, Nevada. Annual Meeting of the American Geophysical Union

Nadelhoffer, K.J., Fry, B., 1994. Nirtogen isotope studies in forest ecosystems. In: Lajtha, K., Michener, R.H. (Eds.), Stable Isotopes in Ecology and Environmental Science. Blackwell Scientific Publication, Boston, USA, pp 23-44.

Pancost, R.D., and Sinninghe Damste, J.S., 2003. Carbon isotopic compositions of prokaryotic lipids as tracers of carbon cycling in diverse settings. Chemical Geology, 195:29-58.

Pentecost, A., 2005. Travertine. Springer, Netherlands, 542 pp.

Peters, K.E., Moldowan, J.M., 1993. The biomarker guide: interpreting moleculat fossils in petroleum and ancient sediments. Prentice Hall, Englewood Cliffs, NJ, USA.

Peters, K.E., Walters, C.C., Moldowan, J.M., 2005. Biomarkers and isotopes in the environment and human history. Cambridge University Press, Cambridge, UK.

Ray, P.H., White, D.C., and Brock, T.D., 1971. Effect of temperature on the fatty acid composition of Thermus aquaticus. Journal of Bacteriology, 106 (1); 25-30.

Reading, H.G. (Ed.), 1986. Sedimentary environments and facies. Blackwell Scientific Publications.

Renaut, R.W., and Jones, B., 2001. Role of microorganisms in the formation of travertine and siliceous sinter in hot and boiling springs of the Kenya Rift Valley. GeoCanada, 70-73.

Summons, R.E., Jahnke, L.L., and Simoneit, R.T., 1996. Lipid biomarkers for bacterial ecosystems: studies of cultured organisms, hydrothermal environments and ancient sediments. Evolution of Hydrothermal Ecosystems on Earth (and Mars?) 174-194. Wiley.

Theil, V., Merz-Preib, M., Teitner, J., Michaellis, W., 1997. Biomarker studies on microbial carbonates: extractable lipids of a calcifying cyanobacterial mat (everglades, USA). Facies, 36:163-172.

Waggoner, B. 2002. Molecular palaeontology. In: Encyclopedia of Life Sciences. Vol. 12, pp. 227-232.

Ward, D.M., Panke, S., Kloppel., K.D., Christ, R., and Fredrickson, H., 1994. Complex polar lipids of a hot spring cyanobacterial mat and its cultivated inhabitants. Applied and Environmental Microbiology, 60 (9); 3358-3367.

Wait, R., Carreto, L., Fernanda, M., Ferreira, A.M., and Da Costa, M.S., 1997. Charaterization of

novel long-chain 1,2-diols in *Thermus* species and deomonstration that *Thermus* strains contain both glycerol-linked and diol-linked glycolipids. Journal of Bacteriology, 179 (19); 6154-6162.

Zhang, C.L., Fouke, B.W., Bonheyo, G.T., Peacock, A.D., White, D.C., Huang, Y., and Romanek, C.S., 2004. Lipid biomarkers and carbon-isotopes of modern travertine deposits (Yellowstone National Park, USA): Implications for biogeochemical dynamics in hot-spring systems. Geochemica et Cosmochemica Acta, 68(15):3157-31

Table 1: Geochemical data at Jackson Mountain Hot Spring.

Location	temp °C		pH	
	2004	2006	2004	2006
vent 1	68.8	inactive	7.3	inactive
vent 2	54.3	74.4	7.4	7.4
vent 3	72.6	72.7	7.4	7.3
proximal slope (#3-5)	nd	60.8	nd	6.2
distal slope (#6)	nd	46.9	nd	8.6

nd= no data available

Table 2: Mineralogy of sections at Jackson Mountain Travertine Ridge.

Section		sample id	Wt % Calcite[a]	Wt % Aragonite
Section 1		lily pad (sample #2)	5	95
		sub-green terracettes (sample #5)	4	96
		dry terracettes (sample #7)	2	98
		sub-dry terracettes (sample #8)	2	98
Section 2: exposed layers		A (0-8 cm)	74	26
		B (10-18cm)	97	3
		C (28-41cm)	97	3
		D (50-61 cm)	97	3
		E (91-99 cm)	97	3
		F (109-119 cm)	97	3
Section 2: Cores	1	A (0-10 cm)	64	36
		B (10-20 cm)	78	22
		C (20-35 cm)	76	24
		D (35-45 cm)	97	3
	2	A (0-10 cm)	76	24
		B (10-20 cm)	69	31
		C (20-35 cm)	61	39
		D (35-45 cm)	97	3
Section 4: Representative Samples	exterior lamination	A1	97	3
		A2	97	3
		A3	97	3
		A4	45	55
	microterracettes	B1	6	94
		B2	3	97
		B3	5	95
Section 4: exposed layers		C1	nd	nd
		C2	nd	nd
		C3	11	89
		C4	7	93
		C5	8	92

nd=no data available

Table 3: Phospholipid Fatty Acid of Section 1 active site.

	Facies					
	Vent			Proximal Slope		Distal Slope
Sample #	1	2	3	4	5	6
Fatty Acids[a] (mol%)[b]	red streamers (Vent 2)	lily pad (Vent 3)	white streamers	green microterracettes	sub-green microterracettes	orange mat
13:0	-	0.22	-	-	-	0.57
14:0	-	0.28	0.33	0.26	-	0.57
15:1ω4	-	-	-	-	-	-
i15:0	3.35	2.92	2.30	1.77	6.35	2.77
a15:0	-	0.72	0.33	-	-	0.37
15:0	-	0.57	-	0.60	7.94	0.55
i16:0	4.24	3.61	1.88	2.50	6.02	1.93
16:1ω7c	-	-	-	-	-	0.70
16:1ω7t	-	0.65	0.74	1.39	1.77	7.89
16:0	4.19	29.97	38.13	36.20	23.59	42.84
17:0 (14 methyl)	-	-	-	-	1.23	1.91
i17:0	11.05	3.79	3.20	3.00	10.21	0.78
17:0 cyc	-	1.12	0.56	0.30	2.30	0.30
17:1ω6c	-	-	0.22	1.03	-	0.44
17:0	-	1.09	0.82	1.43	6.80	0.72
16:0, 2-OH	2.97	0.27	0.26	-	-	-
i18:0	-	0.47	0.18	0.22	-	-
18:2ω6c	-	0.93	-	0.29	2.03	4.05
18:1ω9c	4.05	10.56	14.16	15.77	4.03	17.24
18:1ω7c	1.01	0.66	0.59	0.61	-	3.55
18:1ω7t	1.53	0.51	0.83	0.55	-	-
18:1ω5c	-	2.22	0.48	0.87	-	0.72
18:0	14.73	28.48	28.91	24.63	10.04	6.93
19:0cyc	-	1.80	0.93	2.84	3.18	0.34
20:1ω9c	38.41	1.22	1.00	0.73	1.27	0.34
20:1ω9t	2.45	0.25	0.19	0.33	-	-
20:2	4.32	3.35	1.87	3.19	5.08	-
unknown	7.70	4.34	2.10	1.47	8.15	4.49
Total mol %	100.00	100.00	100.00	100.00	100.00	100.00
Total FAME ug/g sample	36.04	310.17	303.72	439.24	8.60	1146.10

(-)=not detected in sample

[a] FAME identification based on retention times in comparison of reference compounds and mass spectra (≥97 % match).

[b] quanitification of mol % calculated using internal standards of known concentration.

Table 4: Phospholipid Fatty Acid of Section 1 recently active site.

	Facies			
	Proximal Slope			
Sample #	7	8	9	10
Fatty Acids[a] (mol%)[b]	dry microterracettes	sub-dry microterracettes	leathery mat	sub-leathery mat
13:0	-	-	-	1.22
14:0	-	-	-	0.82
15:1ω4	12.28	-	-	0.80
i15:0	20.28	10.90	4.36	4.16
a15:0	2.95	-	1.16	2.47
15:0	-	-	-	0.58
i16:0	5.24	11.15	1.80	2.06
16:1ω7c	-	-	3.87	1.06
16:1ω7t	6.52	4.42	8.62	9.91
16:0	8.39	18.95	17.17	21.63
17:0 (14 methyl)	-	-	15.87	2.46
i17:0	4.82	14.13	2.37	2.40
17:0 cyc	-	3.85	-	0.81
17:1ω6c	-	-	-	-
17:0	-	-	-	0.72
16:0, 2-OH	-	-	-	-
i18:0	-	-	-	-
18:2ω6c	-	-	-	6.49
18:1ω9c	3.83	-	16.03	10.78
18:1ω7c	16.10	4.38	11.37	17.05
18:1ω7t	-	-	-	-
18:1ω5c	-	-	6.89	3.21
18:0	2.38	9.27	2.49	4.33
19:0cyc	-	-	-	2.17
20:1ω9c	-	-	-	-
20:1ω9t	-	-	-	-
20:2	9.23	12.65	-	-
unknown[c]	7.98	10.30	8.01	4.87
Total mol %	100.00	100.00	100.00	100.00
Total FAME ug/g sample	6.64	3.74	170.47	84.77

(-)=not detected in sample

[a] FAME identification based on retention times in comparison of reference compounds and mass spectra (≥97 % match).

[b] quanitification of mol % calculated using internal standards of known concentration.

Table 5: Hopanoid biomarkers of Section 1 active and recently active sites.

	Samples				
		Active		Recently Active	
Sample #	2	4	5	7	9
BHP[a] (ug/g of sample)	lily pad (vent 3)	green terracettes	sub-green terracettes	dry terracettes	leathery mat
2-methylbishomohopanol	-	-	0.03	-	0.46
bishomohopanol	-	-	0.05	0.03	3.30

(-) = not detected in sample

[a] Identification of bacteriohopanes were based on retention times and mass spectra in comparison to reference standards of acetate acetate derivitized BHP's extracted from P. luridium (provided by Roger Summons and Linda Jahnke).

Table 6: Hydrocarbon biomarkers Section 1 active site.

Sample #	Facies					
	Vent			Proximal Slope		Distal Slope
	1	2	3	4	5	6
Hydrocarbons[a] (mol%)[b]	redstreamers (vent 2)	lily pad (vent 3)	white streamers	green microterracettes	sub-green microterracettes	orange mat
8-heptadecene	nd	-	-	-	-	4.04
3-heptadecene	nd	-	-	-	1.24	3.68
heptadecane	nd	73.02	67.42	48.56	3.06	46.89
7-methyl heptadecane	nd	26.98	7.55	27.07	1.29	18.13
5-nonadecene	nd	-	-	-	2.67	-
phytane	nd	-	4.67	-	1.75	-
squalene	nd	-	-	-	2.46	-
total unknowns	nd	0.00	20.36	24.37	87.53	27.25
total mol %	nd	100.00	100.00	100.00	100.00	100.00
total hydro ug/g sample	nd	9.03	28.85	2.90	2.55	87.44

(-) = not detected in sample

nd=no data, limited biomass available

[a] Hydrocarbons identification based on retention times in comparison of reference compounds and mass spectra (≥97 % match). Refer to methods section for details.

[b] quanitification of mol % calculated using internal standards of known concentration.

Table7: Hydrocarbon biomarkers Section 1 recently active sites.

Sample #	Facies			
	Proximal Slope			
	7	8	9	10
Hydrocarbons[a] (mol%)[b]	dry microterracettes	sub-dry microterracettes	leathery mat	sub-leathery mat
8-heptadecene	1.66	-	7.19	4.18
3-heptadecene	2.01	-	15.55	17.69
heptadecane	42.89	12.98	56.28	34.00
7-methyl heptadecane	6.64	-	4.32	31.86
5-nonadecene	0.75	-	-	6.33
phytane	0.63	7.23	-	-
squalene	0.87	10.01	-	-
total unknown	44.54	69.78	16.66	5.93
total mol %	100.00	100.00	100.00	100.00
total hydro ug/g of sample	14.31	0.72	50.29	41.66

(-) = not detected in sample

[a] Hydrocarbons identification based on retention times in comparison of reference compounds and mass spectra (≥97 % match). Refer to methods section for details.

[b] quanitification of mol % calculated using internal standards of known concentration.

Table 8: Hydrocarbon biomarkers for Section 2 hand samples.

Hydrocarbons[a] (mol%)[b]	Hand Samples 2A (0-8cm)	2B (10-18cm)	2C (28-41cm)	2D (50-61cm)	2E (91-99cm)	2F (109.2-119.4cm)
8-heptadecene	-	-	-	-	nd	-
3-heptadecene	8.40	9.01	-	5.33	nd	-
1-heptadecene	-	-	-	-	nd	-
heptadecane	8.44	14.09	10.47	11.56	nd	-
7-methyl heptadecane	20.84	17.65	31.43	30.70	nd	-
5-octadecene	-	4.66	-	4.71	nd	-
9-nonadecene	-	5.82	5.25	5.37	nd	-
5-nonadecene	4.23	6.94	6.52	6.61	nd	-
(3/5/9)-eicosene*	-	4.64	8.42	7.08	nd	-
phytane	-	-	-	-	nd	-
squalene	5.26	7.92	7.09	4.70	nd	100.00
unknowns	52.83	29.26	30.82	23.95	nd	0.00
total	100.00	100.00	100.00	100.00	nd	100.00
Total hydro ug/g of sample	0.98	0.70	0.72	1.15	nd	0.08

(-) = not detected in sample

nd= no data available, sample lost during extraction procedure

[a] Hydrocarbons identification based on retention times in comparison of reference compounds and mass spectra (≥97 % match). Refer to methods section for details.

[b] quanitification of mol % calculated using internal standards of known concentration.

Table 9: Hydrocarbon biomarkers for Section 2 core samples.

Hydrocarbons[a] (mol%)[b]	Section 2							
	Core 1				Core 2			
	A (0-10cm)	B (10-20cm)	C (20-35cm)	D (35-45cm)	A (0-10cm)	B (10-20cm)	C (20-35cm)	D (35-45cm)
	mol %	mol %	mol %	mol %	mol %	mol %	mol %	mol %
8-heptadecene	-	-	-	-	-	-	-	-
3-heptadecene	1.98	-	-	2.04	-	-	-	-
1-heptadecene	-	-	-	-	-	-	-	-
heptadecane	5.09	13.83	9.30	5.32	6.50	5.41	5.86	5.61
7-methyl heptadecane	3.63	8.69	6.09	4.09	-	4.72	4.86	6.24
5-octadecene	-	-	-	-	-	-	-	-
9-nonadecene	-	-	-	-	-	-	-	-
5-nonadecene	2.81	9.12	8.81	3.42	4.12	2.47	5.73	3.56
(3/5/9)-eicosene*	2.27	5.85	3.54	2.99	-	-	-	-
phytane	2.46	8.31	-	2.79	-	1.68	3.36	5.97
squalene	4.21	21.75	7.78	-	19.25	25.56	10.95	4.28
unknowns	77.55	32.44	64.49	79.34	70.14	60.16	69.24	74.34
total	100.00	100.00	100.00	100.00	100.00	100.00	100.00	100.00
Total hydro ug/g of sample	1.57	0.32	0.55	0.96	0.31	0.61	0.37	0.30

(-) = not detected in sample

[a] Hydrocarbons identification based on retention times in comparison of reference compounds and mass spectra (≥97 % match). Refer to methods section for details.

[b] quanitification of mol % calculated using internal standards of known concentration.

Table 10: Hydrocarbon biomarkers for facies at Section 4.

Hydrocarbons[a] (mol%)[b]	Morphology						
	exterior lamination				microterracettes		
	A1	A2	A3	A4	B1	B2	B3
8-heptadecene	-	-	1.32	-	4.39	-	-
3-heptadecene	-	7.75	3.91	16.20	4.98	7.46	61.41
1-heptadecene	7.08	-	-	-	-	-	-
heptadecane	8.83	21.48	12.38	15.15	17.62	13.72	27.01
7-methyl heptadecane	-	17.86	32.97	25.88	29.71	30.03	-
5-octadecene	-	-	-	6.38	3.61	4.47	5.17
9-nonadecene	-	-	2.76	-	7.05	11.59	-
5-nonadecene	3.10	-	4.48	9.91	6.87	2.87	4.07
(3/5/9)-eicosene*	-	-	6.81	6.92	7.53	-	-
phytane	3.07	-	1.90	6.42	-	-	-
squalene	10.21	5.14	2.42	3.27	4.03	4.83	2.34
unknowns	67.71	47.77	31.06	9.87	14.22	25.03	0.00
total	100.00	100.00	100.00	100.00	100.00	100.00	100.00
Total hydro ug/g of sample	0.72	0.76	1.79	0.68	1.13	0.73	0.76

(-) = not detected in sample

[a] Hydrocarbons identification based on retention times in comparison of reference compounds and mass spectra (≥97 % match). Refer to methods section for details.

[b] quanitification of mol % calculated using internal standards of known concentration.

Table 11: Hydrocarbon biomarkers from Section 4 exposed layers.

Hydrocarbons[a] (mol%)[b]	exposed layers C1 (0-8 cm)	C2 (10-18 cm)	C3 (28-41 cm)	C4 (51-61 cm)	C5 (91-99 cm)
8-heptadecene	-	-	-	nd	-
3-heptadecene	-	-	-	nd	-
1-heptadecene	-	-	-	nd	-
heptadecane	-	59.12	38.23	nd	14.56
7-methyl heptadecane	-	-	-	nd	-
5-octadecene	-	22.60	-	nd	9.45
9-nonadecene	-	-	-	nd	-
5-nonadecene	-	-	-	nd	22.93
(3/5/9)-eicosene*	-	-	-	nd	-
phytane	-	-	-	nd	-
squalene	100.00	-	16.92	nd	9.04
unknowns	0.00	18.28	44.85	nd	44.01
total	100.00	100.00	100.00	nd	100.00
Total hydro ug/g of sample	0.05	0.09	0.11	nd	0.37

(-) = not detected in sample

[a] Hydrocarbons identification based on retention times in comparison of reference compounds and mass spectra (≥97 % match). Refer to methods section for details.

[b] quanitification of mol % calculated using internal standards of known concentration.

nd=no data, sample lost during extraction

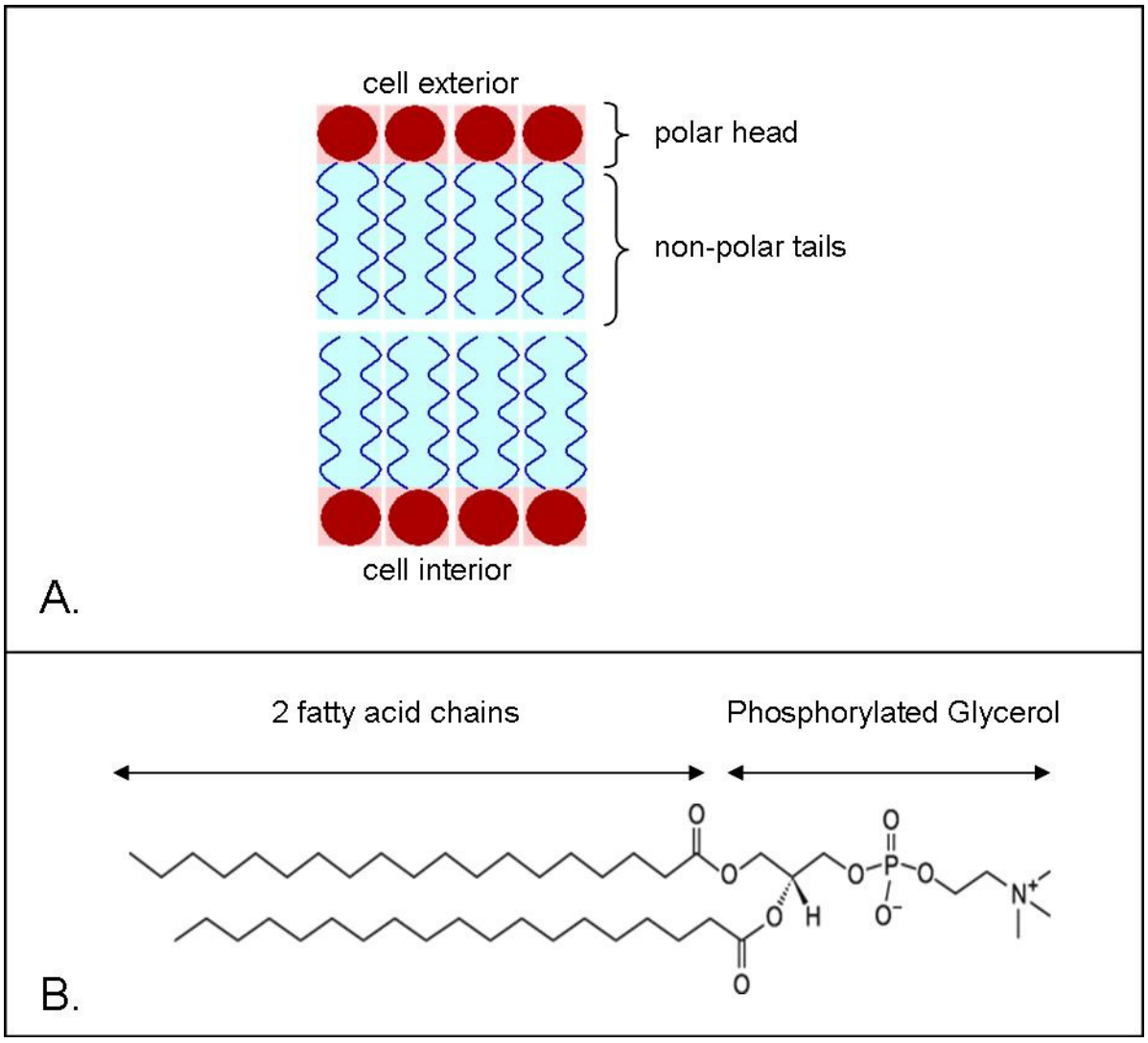

Figure 1: Structure and orientation of phospholipid fatty acid biomarkers. a) organization of lipid bilayer membrane, b) Phospholipid fatty acid molecular structure of 1,2-dinonadecanoyl-sn-glycero-3-phosphocholine,

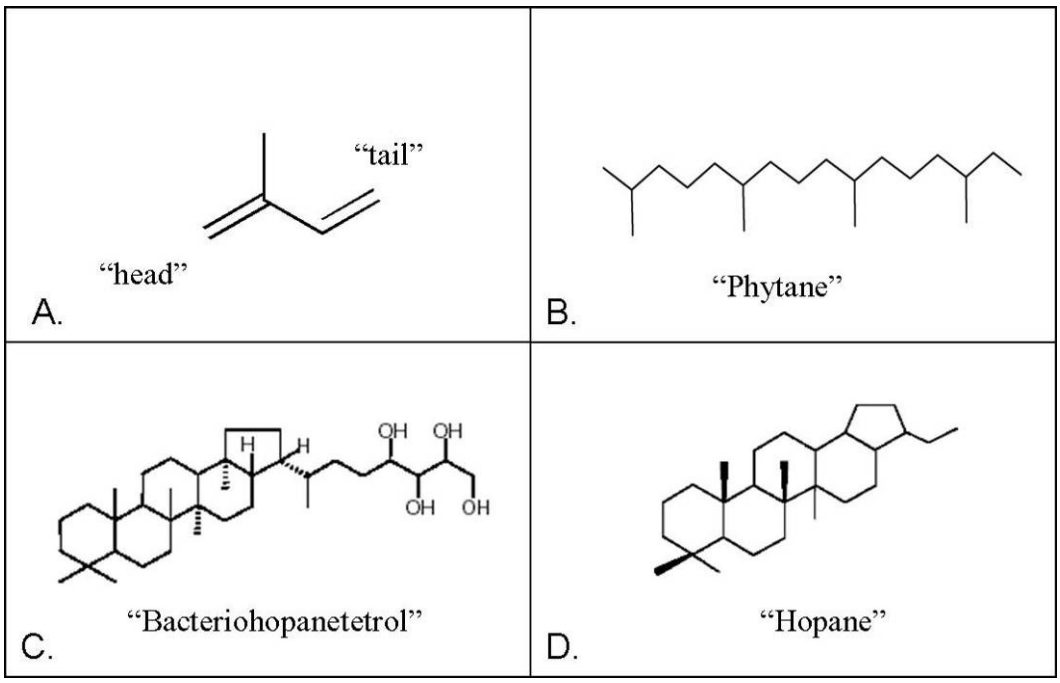

Figure 2: Structure of isoprene unit and common examples. a) isoprene unit, b) the acyclic isoprenoid hydrocarbon phytane, c) the cyclic isoprenoid hydrocarbon bacteriohopantetrol, and d) the geologically stable isoprenoid hydrocarbon hopane.

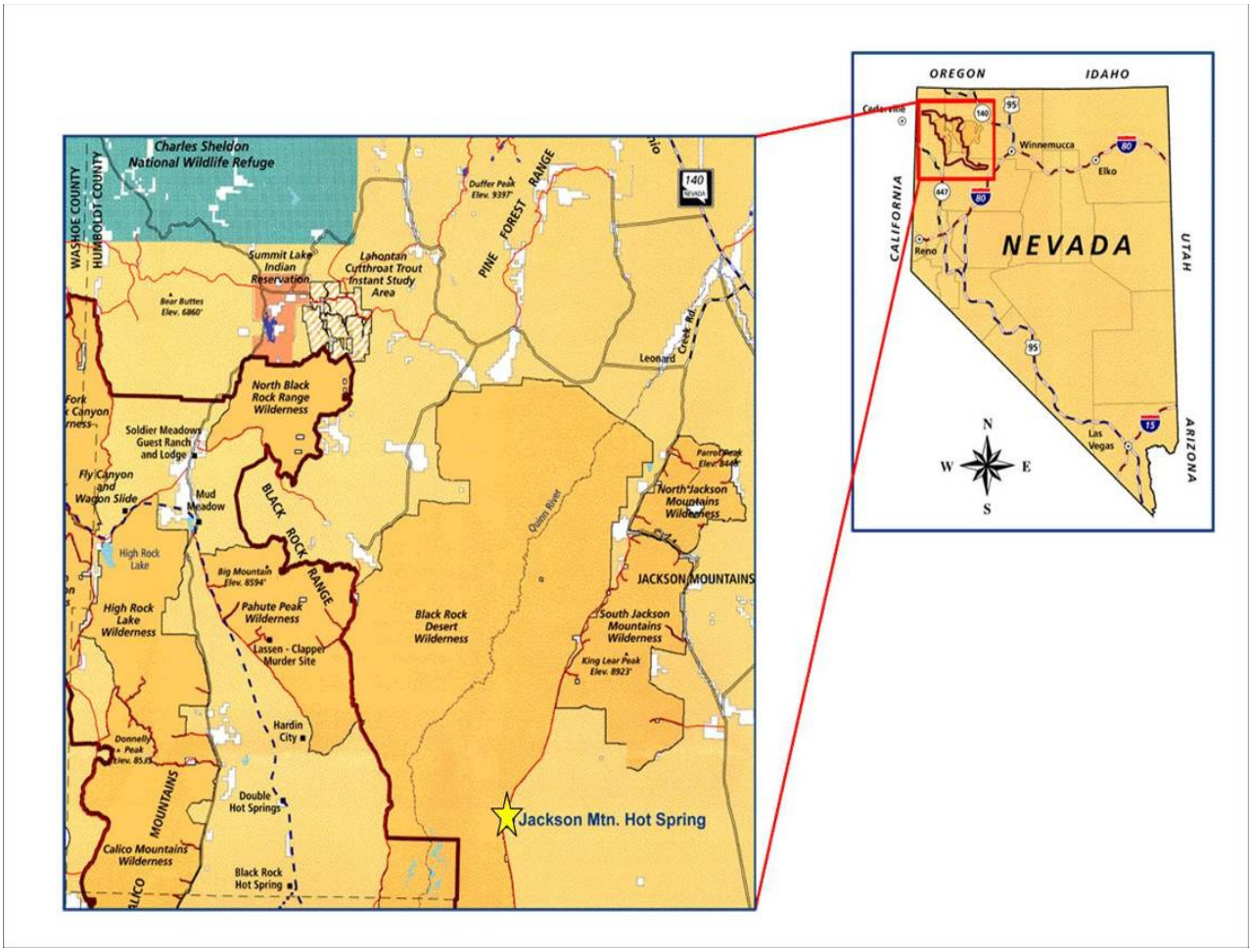

Figure 3: Map showing location of Jackson Mountain Hot Spring (Mills et al., 2004).

Figure 4. Overview of Jackson Mountain Travertine Ridge. a) Section 1, at the western end of the ridge, containing active hot springs, b) view to the east from section 1 of ridge, c) Section 4, at eastern end of ridge.

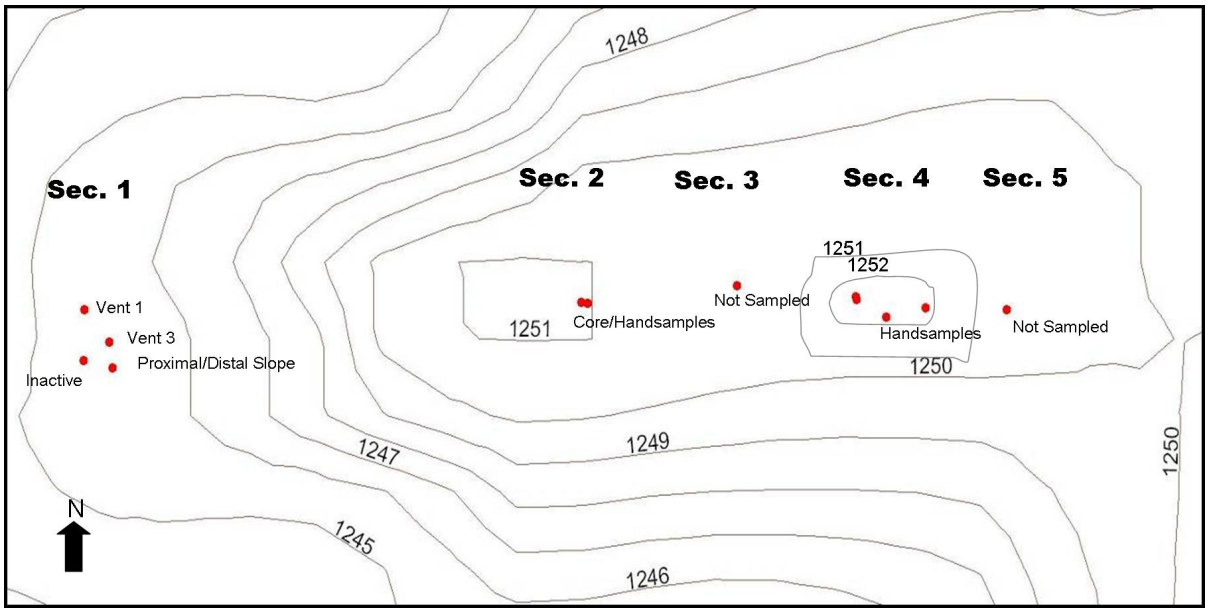

Figure 5: Contour map of Jackson Mountain Travertine Ridge. UTM zone 11, 355529E, 4545834N. Contour units in feet. Red points are representative of sampling locations within sections. Section 3 and 5 were not sampled.

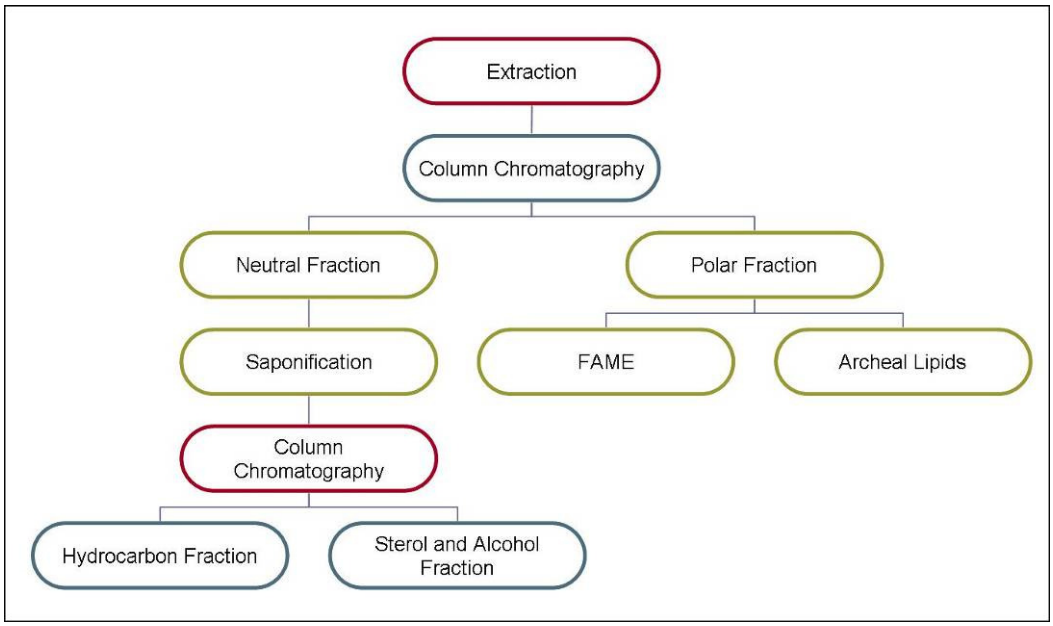

Figure 6. Flow chart for lipid extraction for active mat samples.

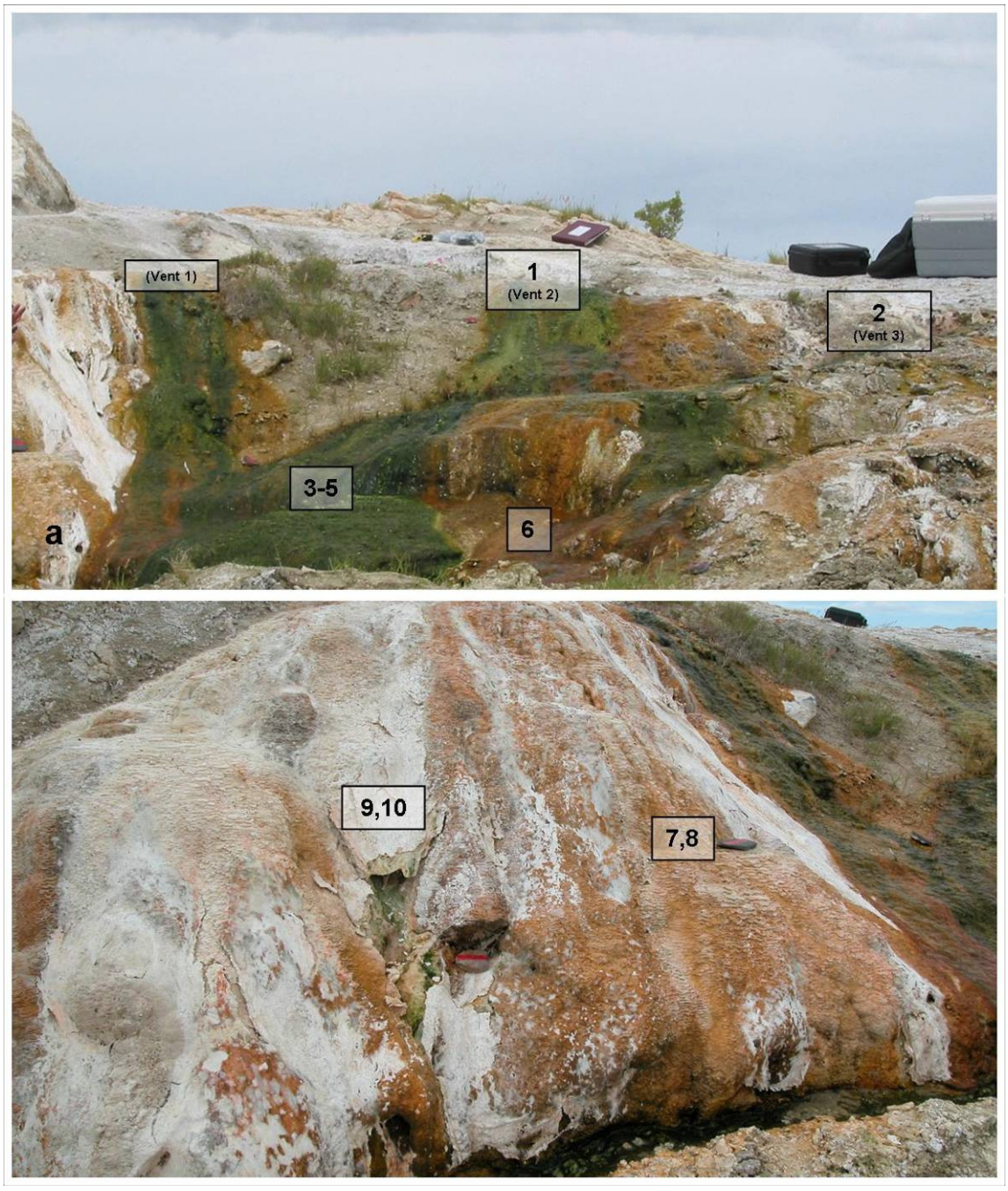

Figure 7. Section 1 sampling locations. a) active hot spring, b) recently active site. Numbers correspond with sample identification. 1. red streamers, 2. lily pad, 3. white streamers, 4. green microterracettes, 5. sub-green microterracettes, 6. orange mat, 7. dry microterracettes, 8. sub-dry microterracettes, 9. leathery mat, 10. sub-leathery mat.

Figure 8: Active hot spring facies and samples. a) vent facies; red streamers #1, b) vent facies; lily pad sample #2, c) proximal slope facies; white streamers on green microterracettes #3, d) proximal slope facies; green microterracettes #4, e) proximal slope facies; sub-green microterracettes #5, f) distal slope facies; orange mat #6.

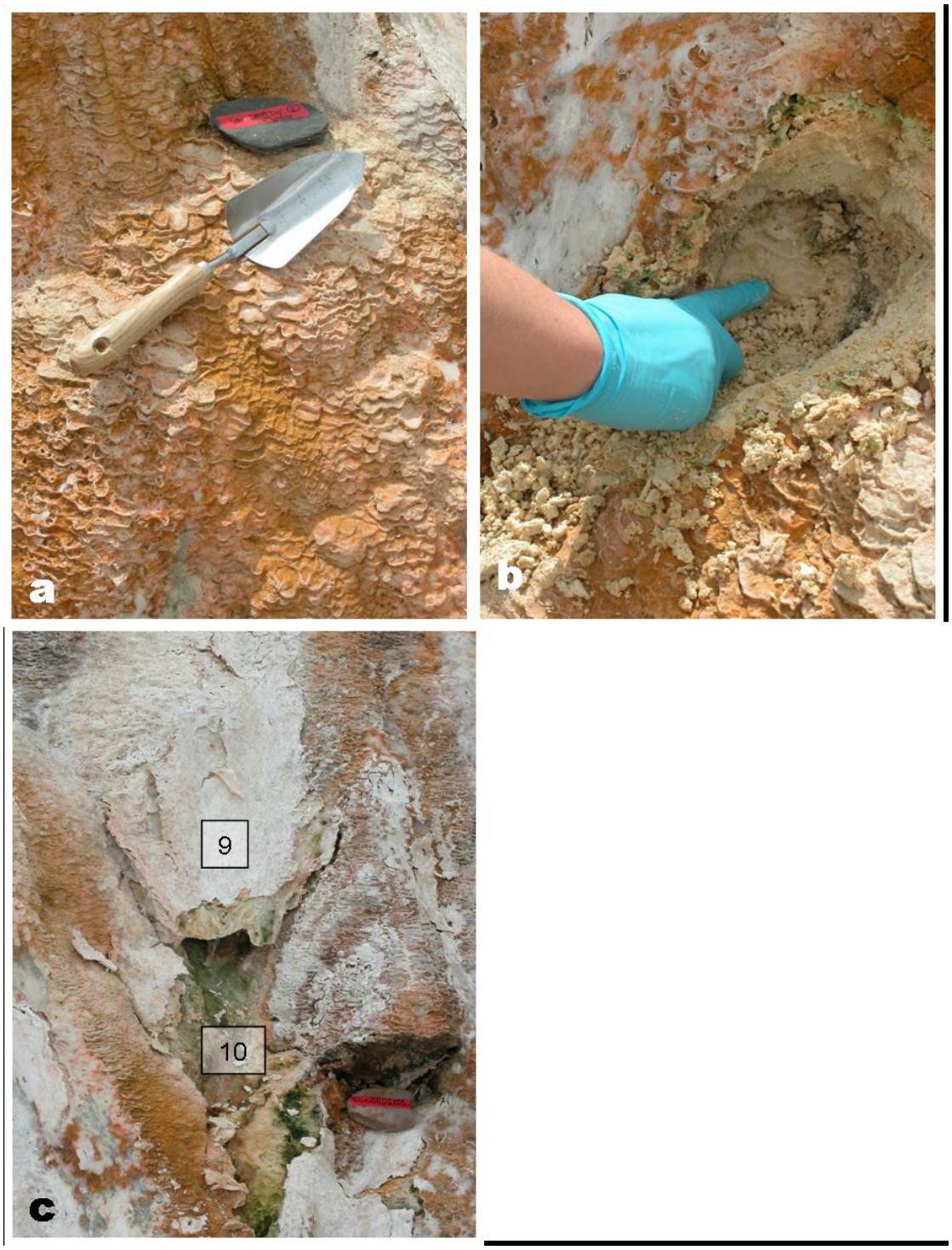

Figure 9: Recently active samples at Section 1. a) dry microterracettes sample # 7, b) sub-dry microterracettes sample # 8 (hand is pointing to green sub layer), c) leathery mat sample #9 and sub-leathery mat sample #10 (a portion of sample #9 was removed to expose sample # 10). Numbers correspond with sample identification.

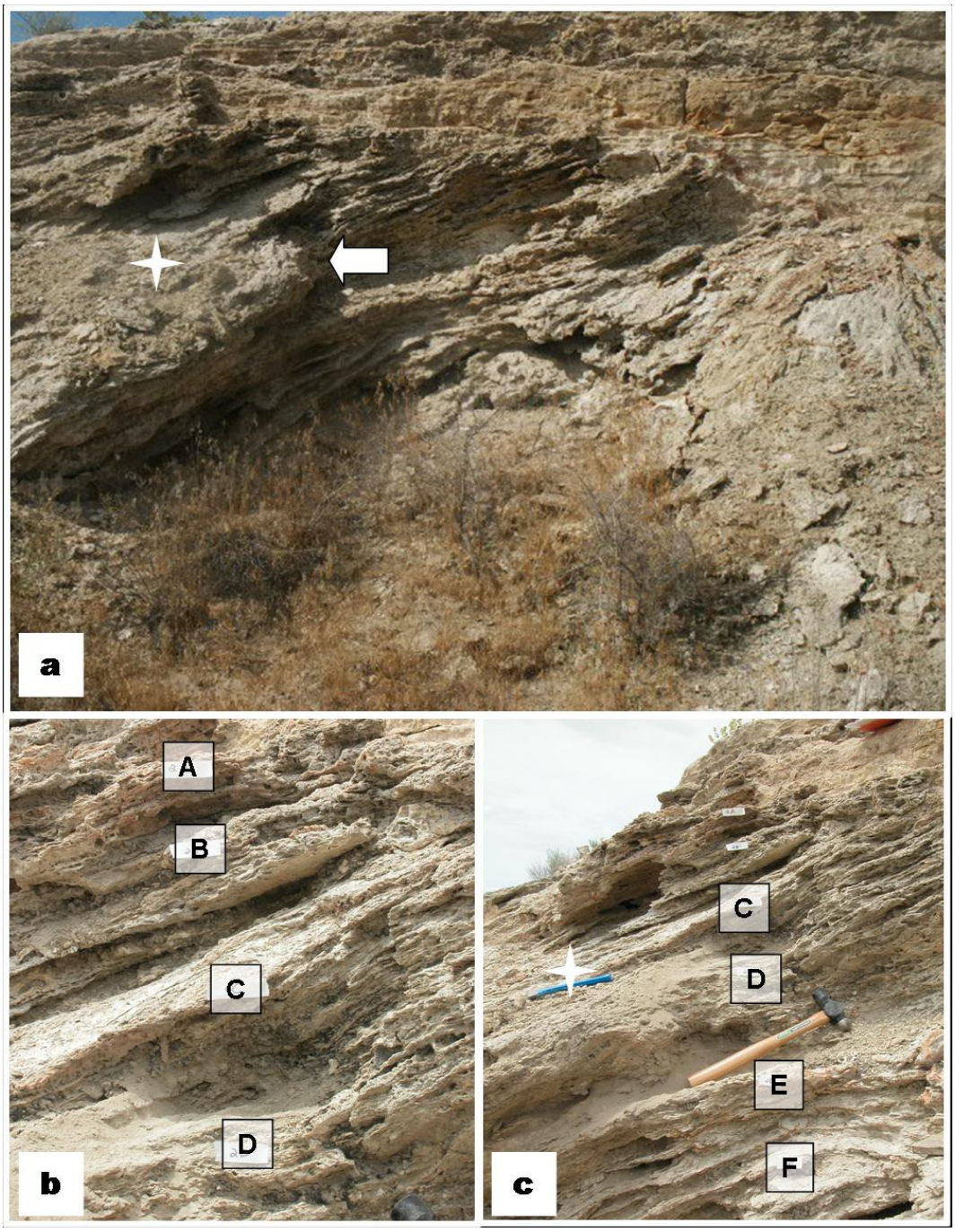

Figure 10: Facies at Section 2. Arrow indicates location of exposed layers. Star indicates location of core samples. Cores were drilled on the surface of layer C. a) overview of Section 2 sampling locations, b) exposed layers A thru D, c) layers E and F.

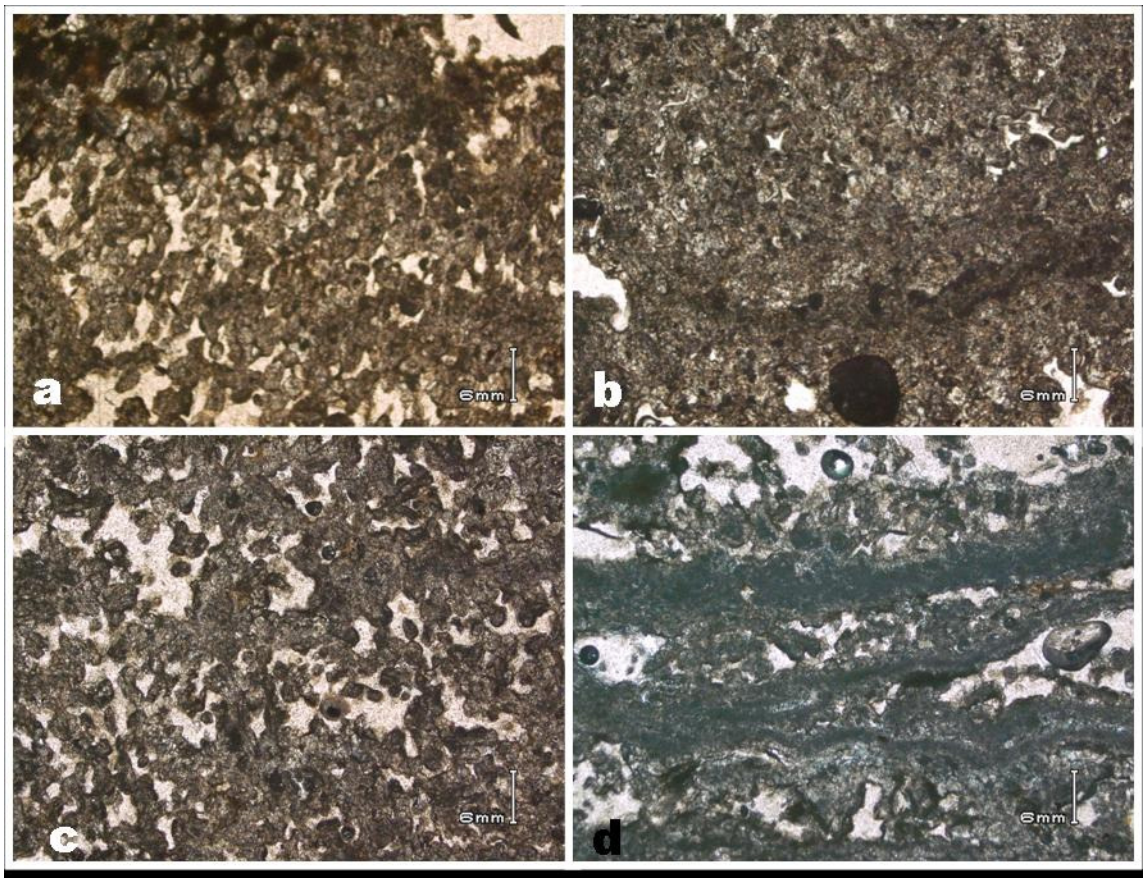

Figure 11: Thin Sections from hand samples at Section 2. Thin sections were taken in reflected light. a) Exposed layer C course grained fenestral fabric. b) Exposed layer C trace laminations. c) Exposed layer D course grained fenestral fabric. d) Exposed layer D trace laminations.

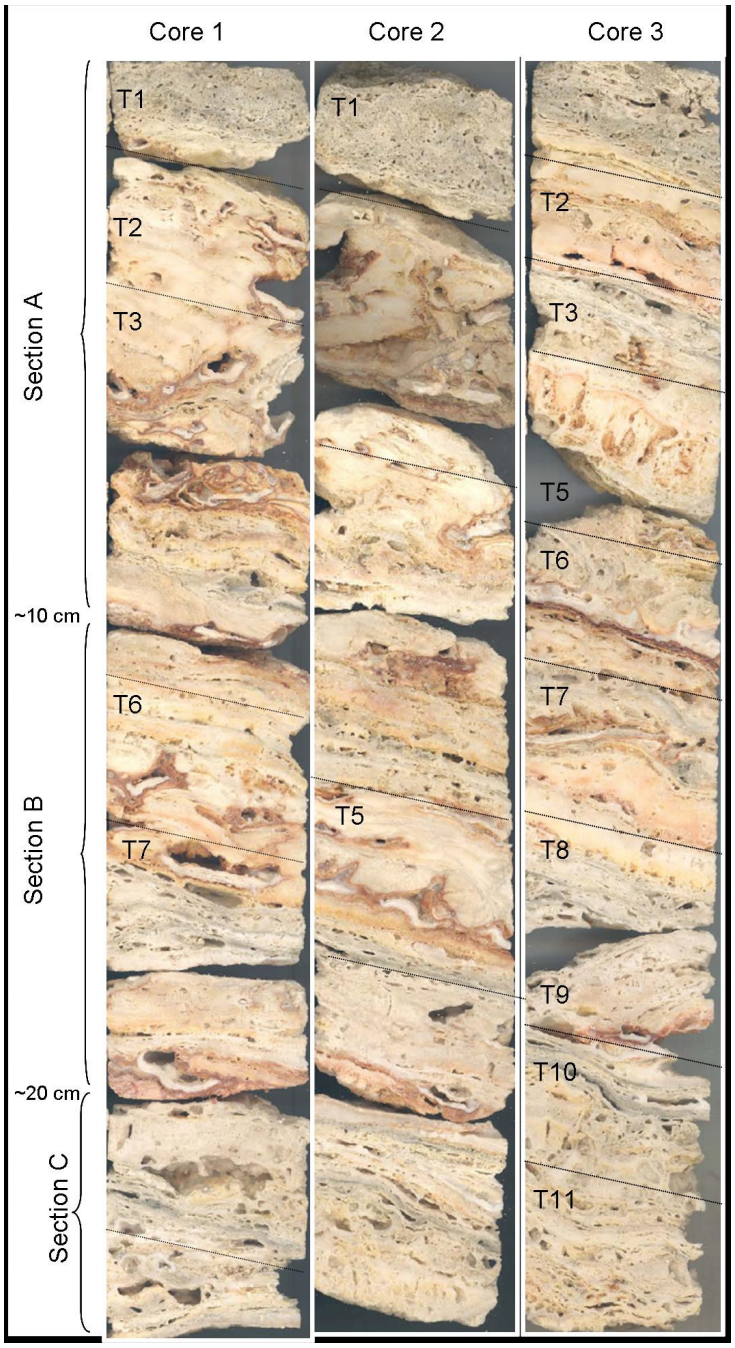

Figure 12. Upper portion of 3 cores from Section 2. Sections represent division of material for analysis. Dashed lines indicate locations were samples were cut for thin sections. T# indicates thin section number for core.

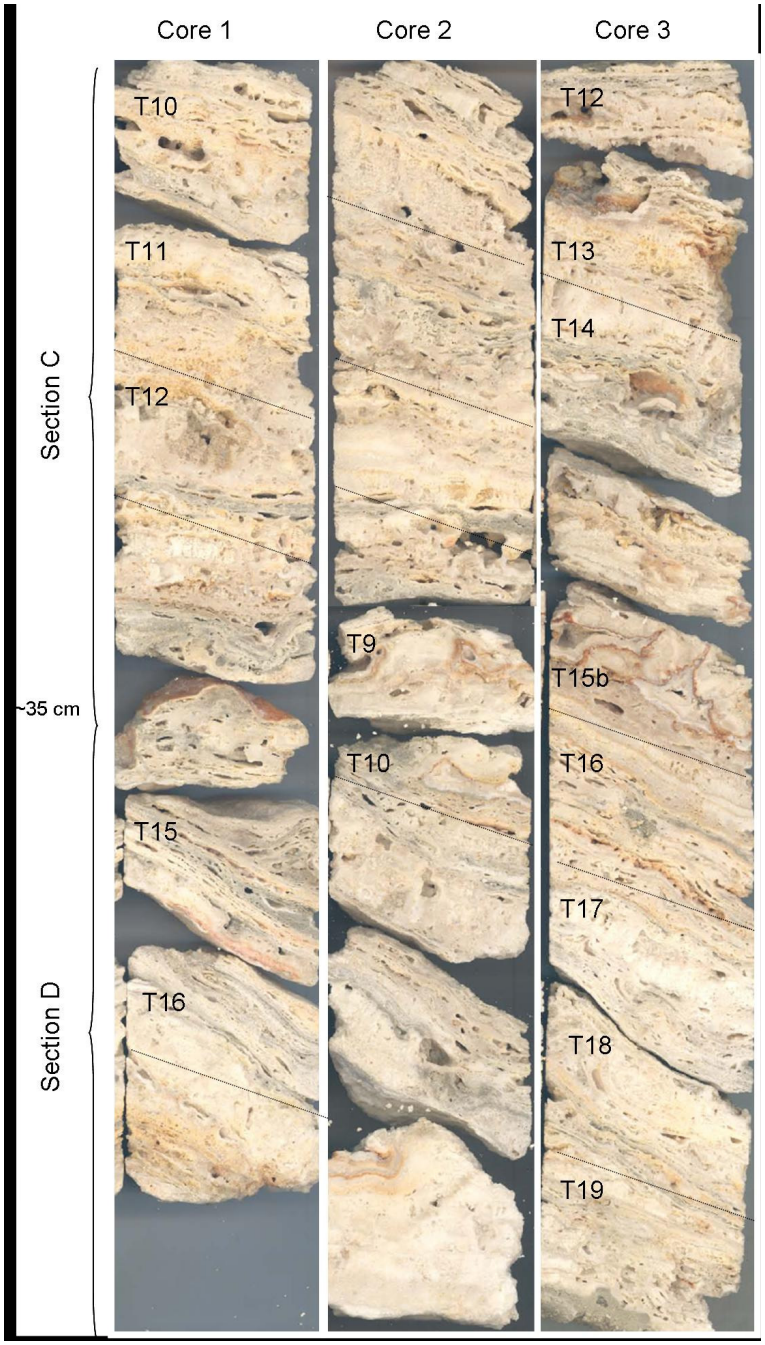

Figure 13: Lower portion of Section 2 core samples. Sections represent division of material for analysis. Dashed lines indicate locations were samples were cut for thin sections. T# indicates thin section number for core.

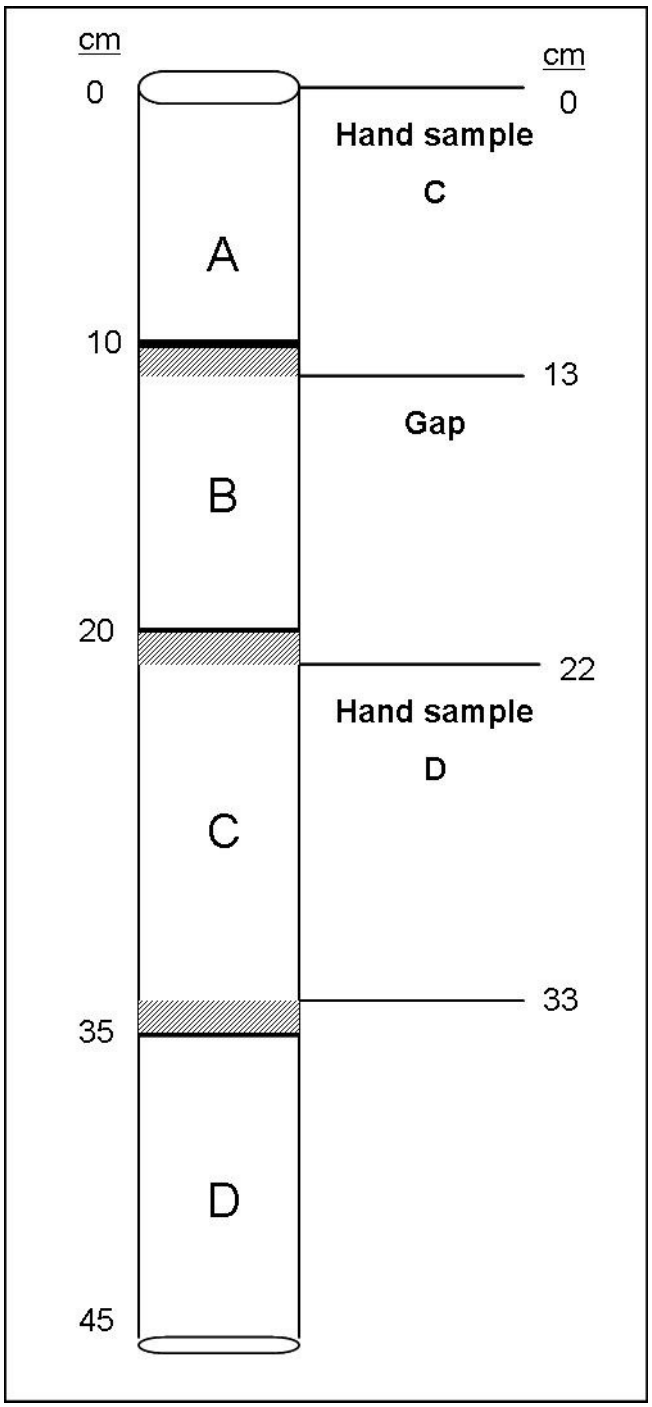

Figure 14: Diagram depicting relationship of core and hand samples.

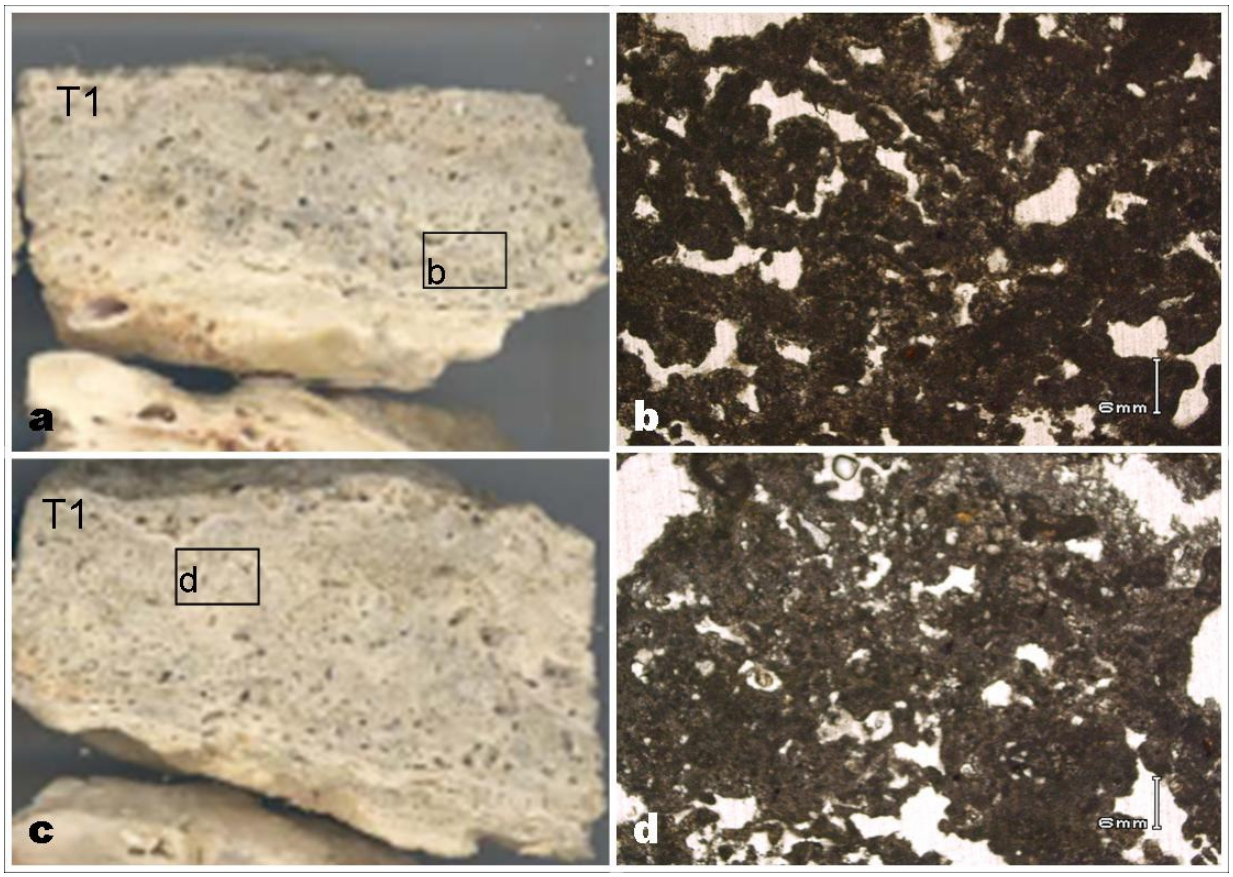

Figure 15: Photographs of cores and thin sections showing fabric of the uppermost portion of cores. Thin sections were taken in reflected light. a) Core 1 T1 with locations of photomicrographs indicated with box, b) example of course grained, fenestral fabric, c) Core 2 T1 with locations of photomicrographs indicated with box, d) example of course grained, fenestral fabric

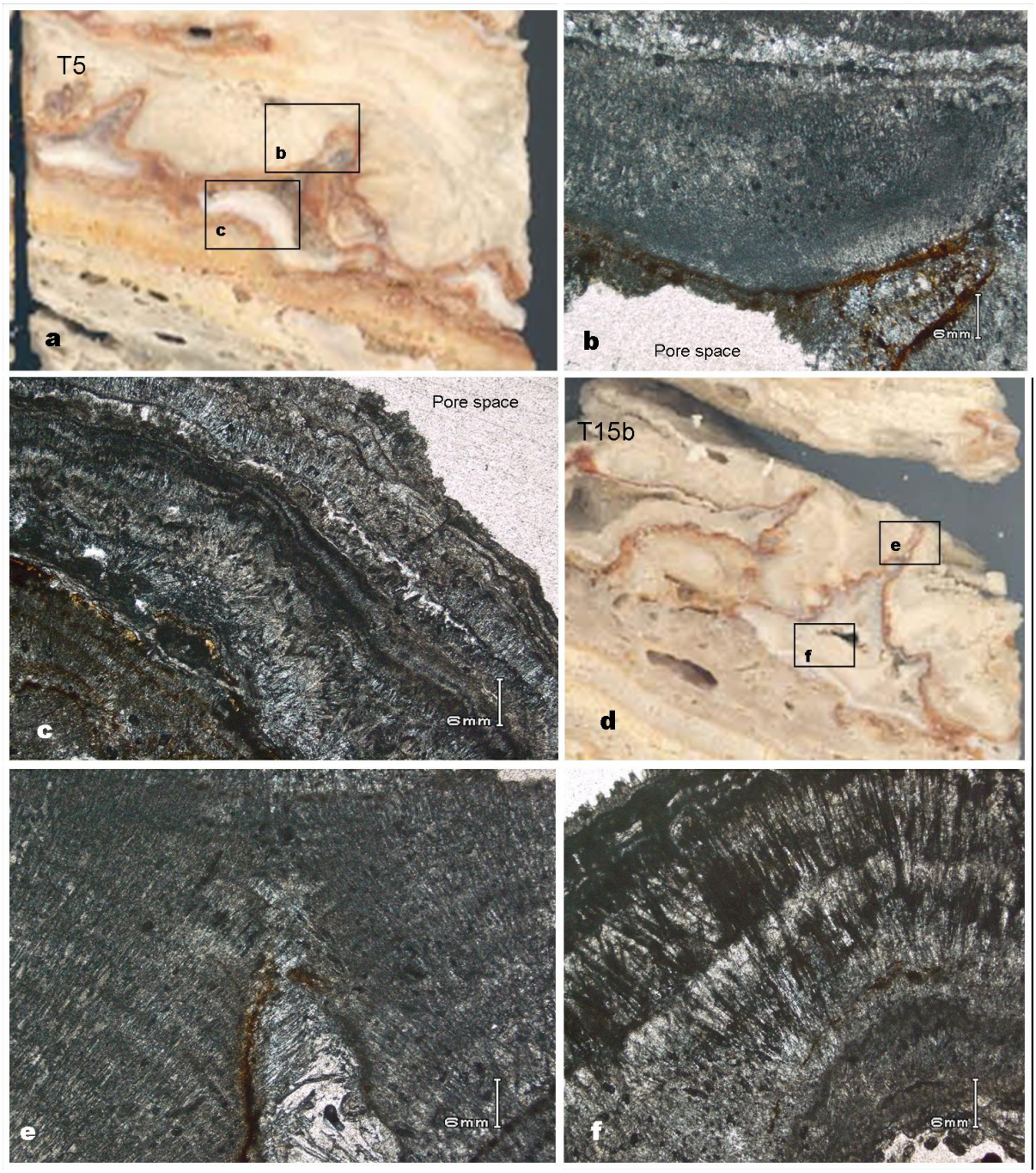

Figure 16: Photographs of core and thin sections showing corrugated bands. Thin sections were taken in reflected light. a) Core 1 T5 with locations of photomicrographs indicated with box, b) example of tubular, branching fabric above orange corrugated bands (inferred microterracettes) with pore space below microterracette in the bottom left corner, c) example of white cement below pore space in top right of photomicrograph, d) Core 3 T15b with locations of photmicrographs noted e. top of microterracette with tubular, branching fabric f. example of pore-filling cement.

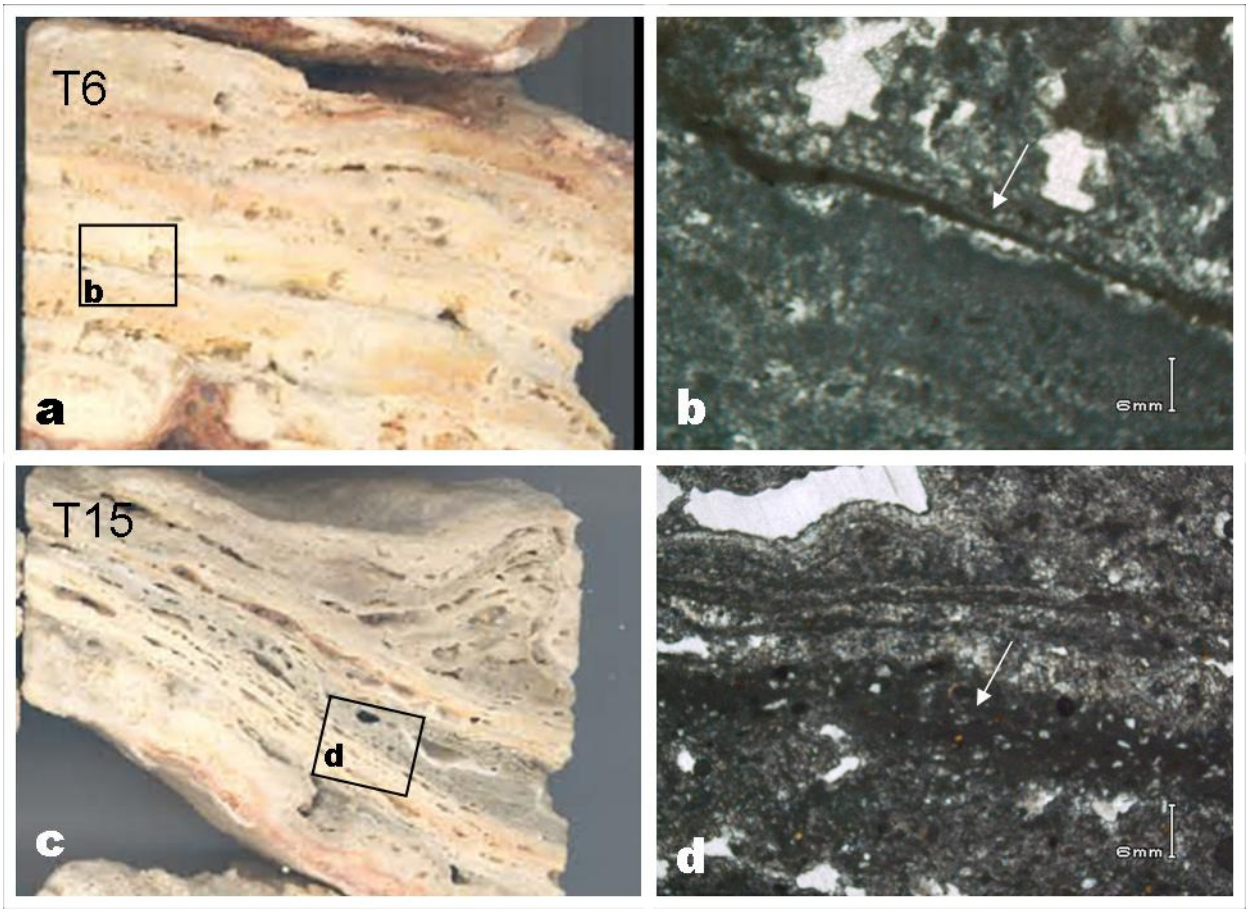

Figure 17. Photographs of thin micrite and carbonate bands in core 1. Thin sections were taken in reflected light. a) alternating layers of thick, coarse grained carbonate bands and thin micrite with thin section location noted (core 1 T6), b) fine grained lamination referred to as thin micrite (arrow) surrounded by coarse grained carbonate bands, c) carbonate bands and thin micrite layers in core 1 T15, d) thin micrite layer with inclusions. White portion at top of b and d is pore space.

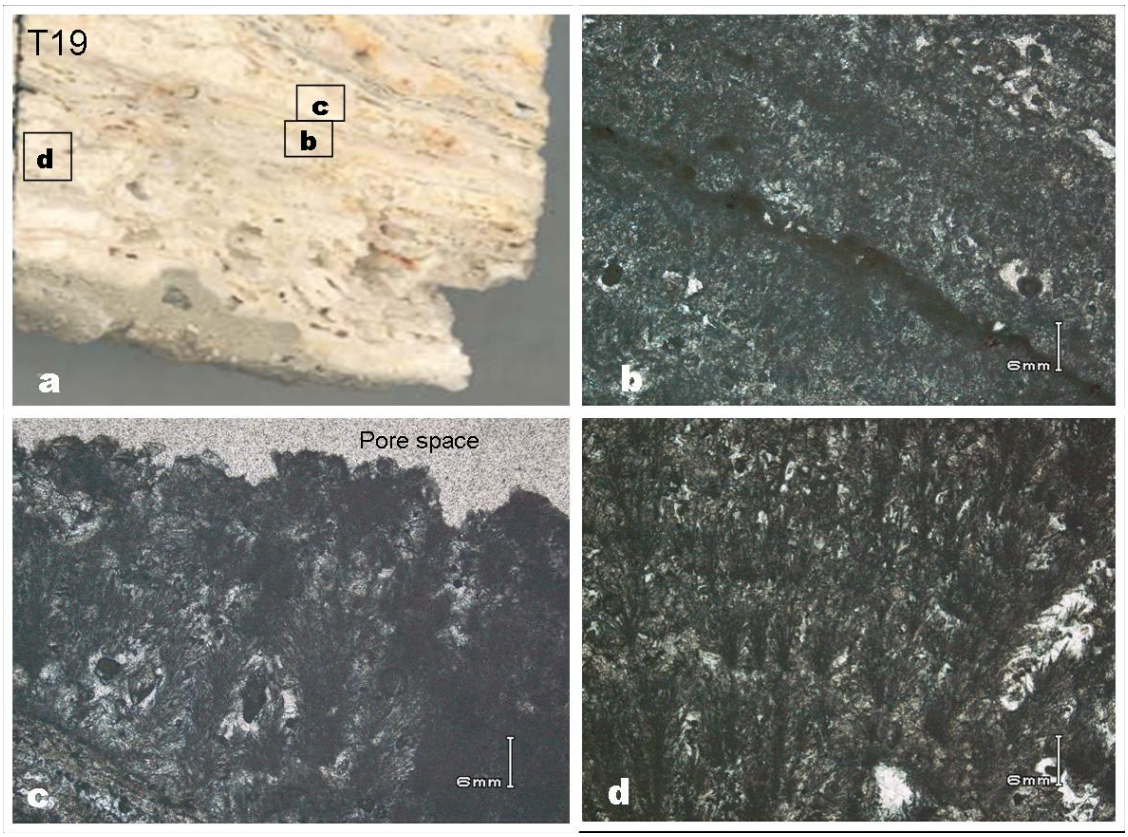

Figure 18: Photographs and thin sections from core 3. Thin sections were taken in reflected light. a) Core 3 T19 with thin sections noted, b) trace laminations, c) dendratic shrubs, d) dendratic shrubs.

Figure 19. Overview of Section 4. Star represents location were exposed layers were sampled. a) view of exposed layers looking north, b) west profile of section 4, c) east profile of section 4. Arrow indicates central fissure ridge.

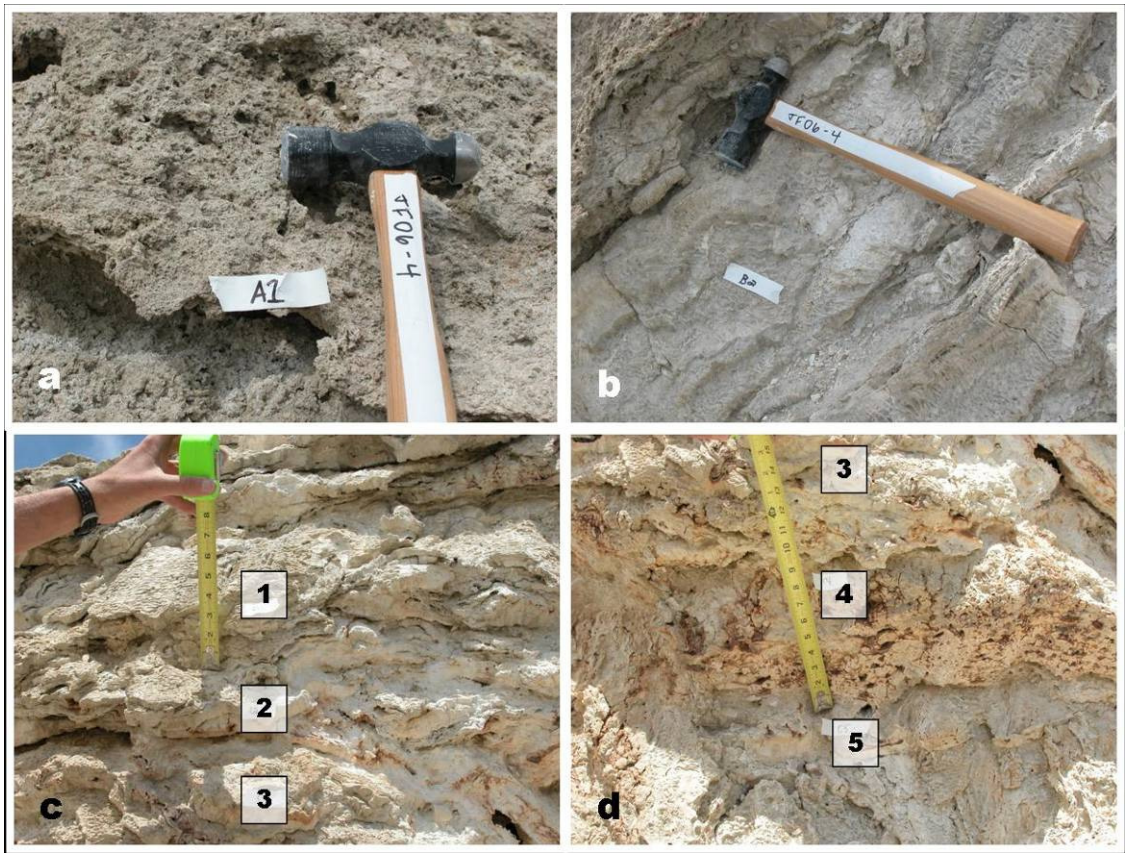

Figure 20: Examples of samples collected from Section 4. a) Representative sample of porous exterior lamination collected at base of Section 4, b) Representative sample of microterracettes collected at base of Section 4, c) exposed layers 1 thru 3 collected at star in Fig. 16a, c) exposed layers 3 thru 5 collected at star in Fig. 16a,c.

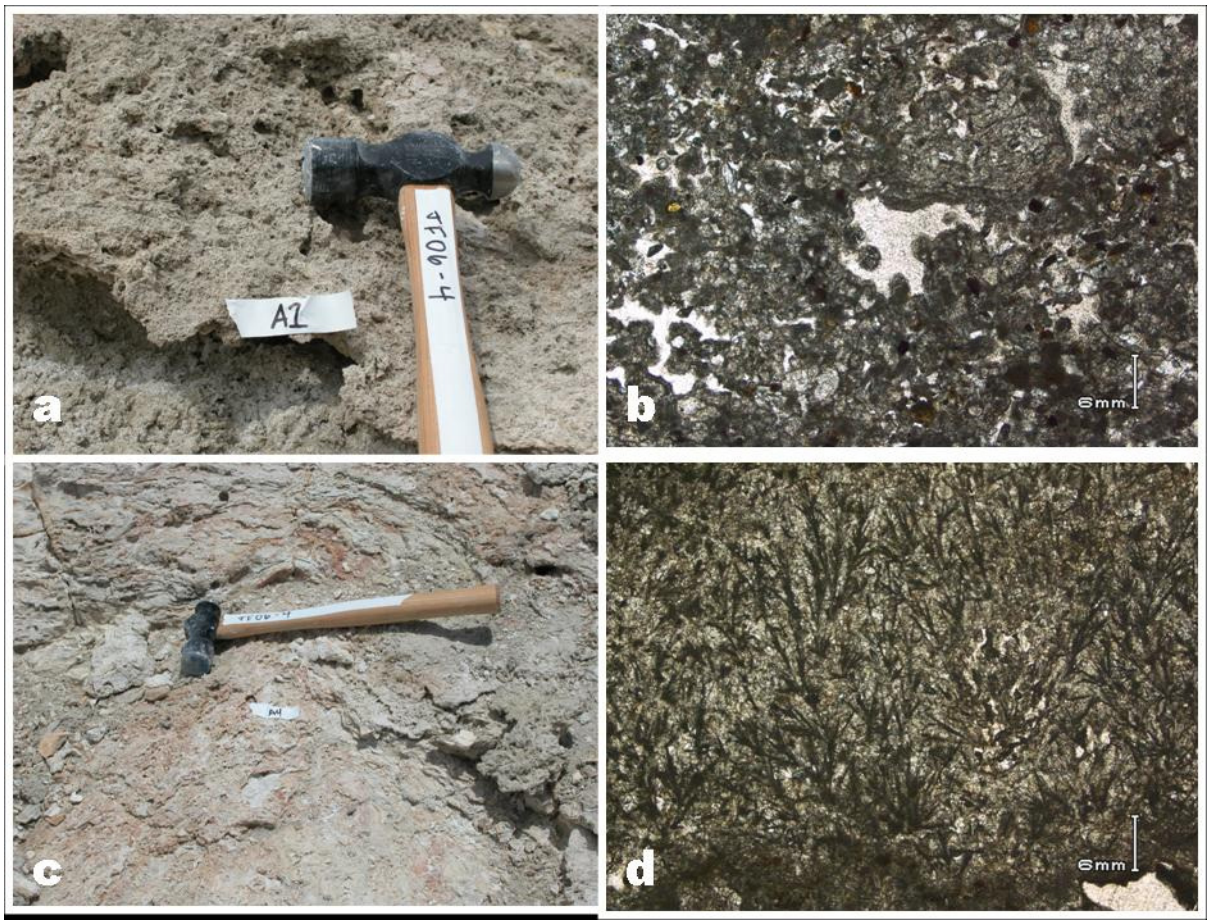

Figure 21: Photographs of exterior laminations and thin sections showing fabrics. Thin sections were taken in reflected light. a) Exterior lamination sample A1, b) course grained, fenestral fabric, c) Exterior lamination sample A4, d) dendritic shrubs fabric in sample A4.

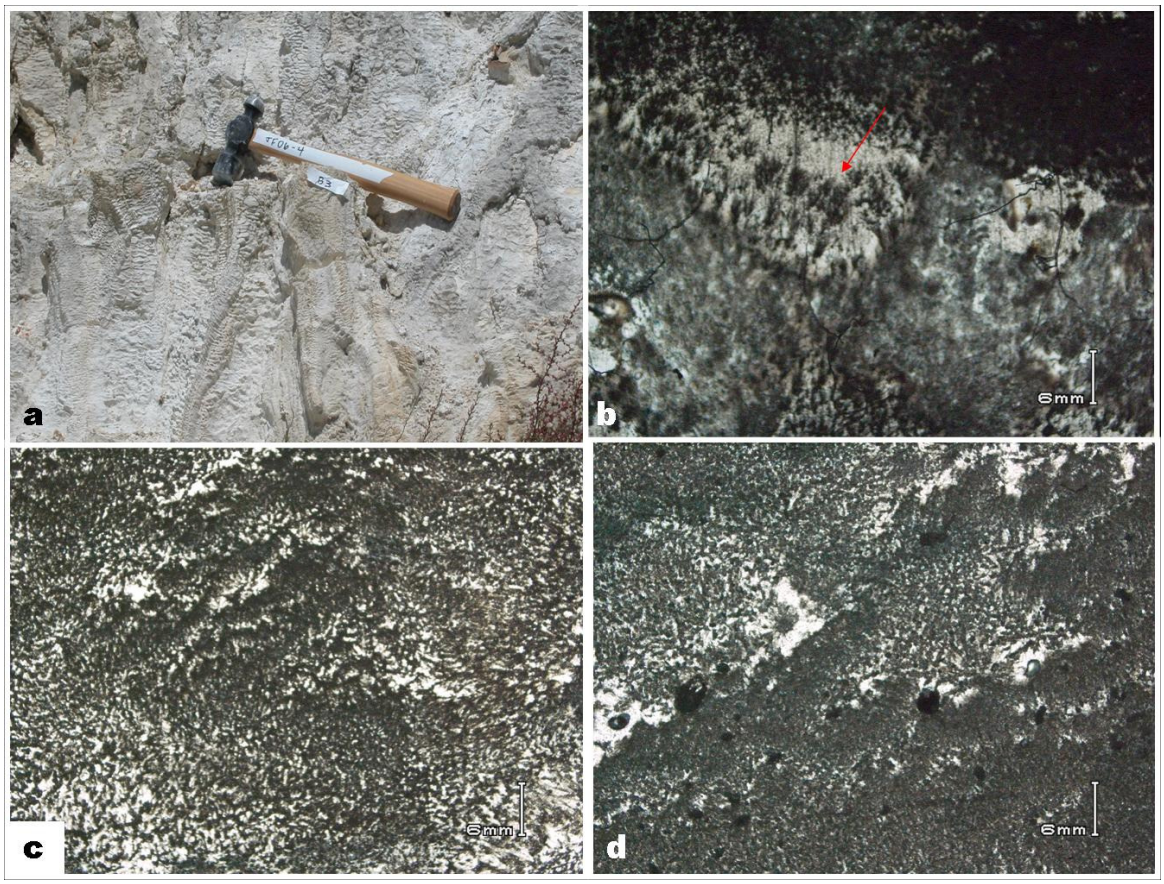

Figure 22: Photographs of microterracettes and thin sections showing fabrics. Thin sections were taken in reflected light. a) Microterracette sample B3, b) dendritic shrubs fabric in sample B3, c) tubular, branching fabric from sample 4B3, d) tubular, branching fabric from sample 4B1.

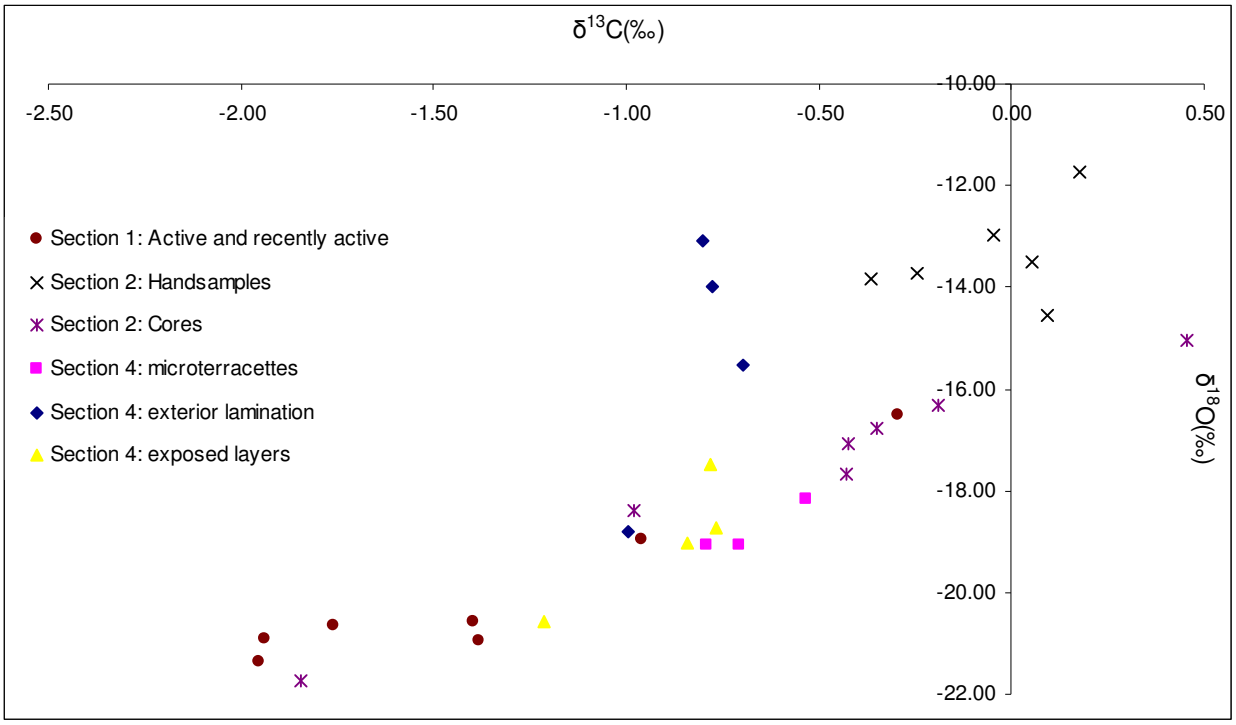

Figure 23: Carbon and oxygen stable isotope composition of bulk active, recently active, and inactive samples at Jackson Mountain Travertine Ridge.

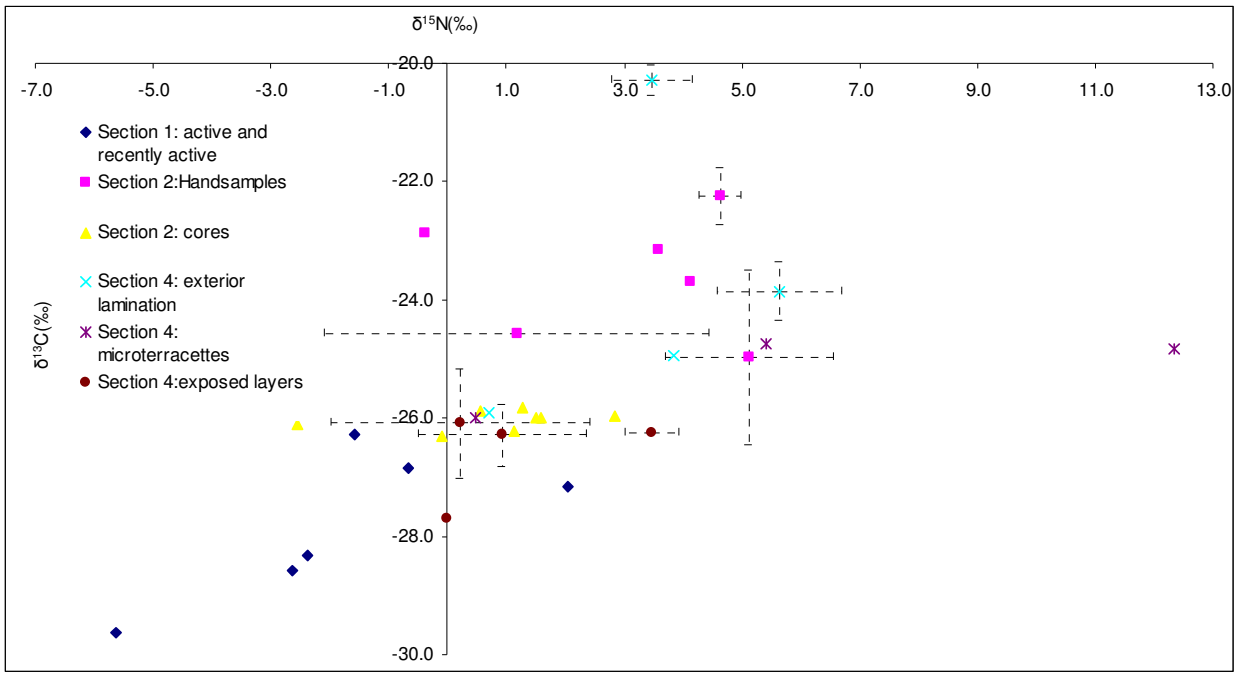

Figure 24: Carbon and nitrogen isotope composition from total organic active, recently active, and inactive samples at Jackson Mountain Travertine Ridge.

APPENDICES

Appendix A: Actual and calculated weight percentages for calcite and aragonite standards.

#	Total Wt. g	Wt. Aragonite g	Wt % Aragonite %	Peak Area aragonite	Wt. Calcite g	Wt % Calcite %	Peak Area calcite	Ic/Ia+Ic	Wt % calcite (+1)	Calculated Wt % Calcite
1	1	0	0	0	1	100.00	182.1	1	101.00	96.9
2	1.0028	0.1001	9.98	2.5	0.9027	90.02	83.8	0.97	91.02	87.0
3	1.0008	0.2002	20.00	9.2	0.8006	80.00	194.5	0.95	81.00	81.9
4	1.0013	0.3011	30.07	10.8	0.7002	69.93	134.9	0.93	70.93	73.5
5	1.0003	0.4003	40.02	12.4	0.6	59.98	85.3	0.87	60.98	60.3
6	1.0014	0.5008	50.01	24.2	0.5006	49.99	108.7	0.82	50.99	49.0
7	1.0022	0.6012	59.99	18.6	0.401	40.01	64.5	0.78	41.01	41.9
8	1.0016	0.7007	69.96	25.5	0.3009	30.04	51.8	0.67	31.04	28.1
9	1.0016	0.8009	79.96	33.8	0.2007	20.04	42.3	0.56	21.04	18.3
10	1.0021	0.9011	89.92	37.9	0.101	10.08	23.9	0.39	11.08	9.7
11	1	1	100.00	40.4	0	0.00	0	0.00	1.00	2.2

Calculated Using y=(6399.0863)/(1+EXP(-(x-2.1038)/0.2644))
Where x=Ic/Ia+Ic, and y=wt % calcite

Appendix B: Sampling locations for 2004 field season (Mills et al., 2004).

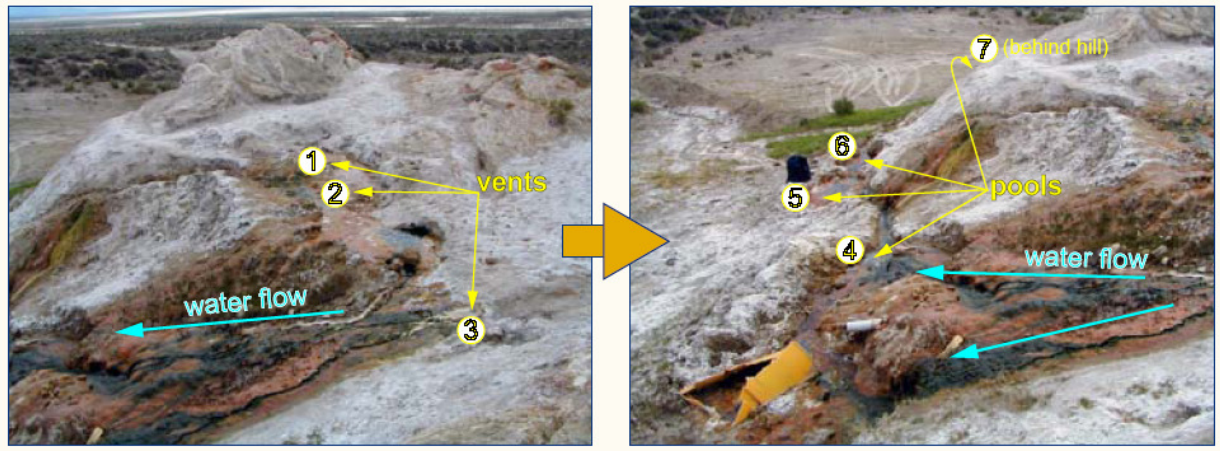

Appendix C: Water chemistry for 2004 field season.

Sample ID	Temp (°C)	pH	cond. (uS/cm)	TDS (mg/L)	DIC (µmol L)	Alk (uM)	Cl (ppb)	Cl (µmol L)	SO4 (ppb)	SO4 (µmol L)	Na (ppb)	K (ppb)	K (µmol L)	Ca (ppb)	Ca (µmol L)	Mg (ppb)	Mg (µmol L)	Mg (ppb)
JMHS 1 m	NA	NA	NA	NA	NA	NA	NA		NA		NA	NA		NA		NA		NA
JMHS 2.1 m	54.3	7.40	5460	2850	30626.2	32385.9	948600	26759	203200	2115	>500,000	28696	734	28771	718	10504	432	11772
JMHS 5.1 m	45.5	8.23	5560	2930	28855.5	32455.1	995300	28076	220300	2293	>500,000	26885	688	18177	454	9526	392	11995
JMHS 6 m	NA	NA	NA	NA	NA	NA	NA		NA		NA	NA		NA		NA		NA
JMHS 7.1 m	60.9	7.00	5600	2960	33632.7	34102.0	1019100	28748	221900	2310	>500,000	29491	754	24500	611	9613	395	11862

*Sampling locations coincide with 2004 sampling locations.

Appendix D: Trace metals from 2004 field season.

Sample location*	Li (ppb)	B (ppb)	Fe (ppb)	Zn (ppb)	Sr (ppb)	As (ppb)	Ti (ppb)	Mn (ppb)	Cu (ppb)	Ga (ppb)	Se (ppb)	Rb (ppb)	Zr (ppb)	Mo (ppb)	Sb (ppb)	Cs (ppb)	Ba (ppb)	W (ppb)	Pb (ppb)
JMHS 1 m	NA	NA	NA	NA	NA	NA	NA	NA	NA	NA	NA	NA	NA	NA	NA	NA	NA	NA	NA
JMHS 2.1 m	230	16846	285	73	3249	1992	9	0	0	0	12	58	0	0	45	90	132	0	1
JMHS 5.1 m	253	17645	201	82	2217	2097	9	0	0	0	12	61	0	0	47	96	134	0	0
JMHS 6 m	NA	NA	NA	NA	NA	NA	NA	NA	NA	NA	NA	NA	NA	NA	NA	NA	NA	NA	NA
JMHS 7.1 m	270	19071	282	165	3380	2251	9	2	0	0	12	64	0	0	50	104	128	0	0

*Sampling locations coincide with 2004 sampling locations.
NA (not available)

Appendix E: Measured and calculated isotopic values from 2004 (Mills et al., 2004).

Sample	$\delta^{13}C_{CaCO3}$	$\delta^{13}C_{CaCO3}$ †	$\delta^{13}C_{dic}$	$\delta^{13}C_{CO2}$ †	P_{CO2} †	$\delta^{13}C_{org}$	$\delta^{13}C_{org}$-$^{13}C_{CO2}$	2004 $\delta^{18}O_w$	2006 $\delta^{18}O_w$	$\delta^{15}N_{toc\text{-}bulk}$	$\delta^{13}C_{toc\text{-}bulk}$	$\delta^{15}N_{toc\text{-}acid}$	$\delta^{13}C_{toc\text{-}acid}$
Location	(‰)	(‰)	(‰)	(‰)	(atm)	(‰)	(‰)	(‰)	(‰)	(‰)	(‰)	(‰)	(‰)
vent 1	-1.85												
vent 2	-0.35	-0.28	-3.8	-8.08	0.1114	-27.35	-19.27	-10.35	-12.35	-3.13	-6.75	-2.73	-27.35
vent 3	-1.84								-12.57				
confluence (vent 2 and 3)									-12.26				
pool 4	-1.61												
pool 5	-1.27	-0.69	-3.2	-8.49	0.0148	-29.54	-21.05	-9.97					
pool 6	-0.74									-2.97	-15.25	-2.57	-29.54
vent 7	-0.49	-0.49	-4.1	-7.49	0.3327	-27.27	-19.78	-10.68		-1.93	-5.40	-1.90	-27.27

† calculated value, see Mills et al. 2004 for details.

2004 sampling locations do not correspond to 2006 sampling locations.

Appendix F: Hach kit analyses from 2006 field season.

Sample ID	DO (ppm)	SO_4^{2-} (ppm)	S^{2-} (ppm)	NO_2^- (ppm N)	NO_3^- (ppm N)	NH_4^+ (ppm N)	Fe^{total} (ppm)	Fe^{2+} (ppm)	SiO_2 (ppm)	PO_4^{3-} (ppm)
red streamers (#1)	53	220	0.02	0.074	38.2	0.55	0.12	0.01	72.4	1.13
lily pad (#2)	198	160	0.04	0.035	35.0	0.60	0.03	0.00	80.7	0.91
green terracettes (#4)	5.4	120	0.02	0.037	28.6	0.54	0.01	0.02	58.4	2.94
orange mat (#6)	NA	NA	NA	NA	NA	NA	NA	NA	NA	NA

*Sampling locations coincide with 2006 field season.

Appendix G: Bulk carbon and oxygen isotope compositions of active and inactive samples.

Section	Sample Description	ID	$\delta^{13}C$ (‰)	$\delta^{18}O$ (‰)	Paleo-temperature* (˚C)
1	Vent	lily pads (#2)	-1.95	-21.37	78
1	Proximal Slope	white streamers (#3)	-0.30	-16.52	47
1	Proximal Slope	green terracettes (#4)	-1.94	-20.89	75
1	Proximal Slope	sub-green terracettes (#5)	-1.76	-20.65	73
1	Proximal Slope	dry terracettes (#7)	-1.40	-20.57	72
1	Proximal Slope	sub-dry terracettes (#8)	-1.38	-20.94	75
1	Proximal Slope	leathery mat (#9)	-0.96	-18.96	62
2	Handsample	2A	0.05	-13.50	31
2	Handsample	2B	0.18	-11.71	22
2	Handsample	2C	-0.36	-13.85	32
2	Handsample	2D	-0.05	-12.98	28
2	Handsample	2E	0.09	-14.57	36
2	Handsample	2F	-0.25	-13.73	32
2	Core 1	Section: A	-0.19	-16.32	46
2	Core 1	Section: B	-1.84	-21.73	80
2	Core 1	Section: C	nd	nd	nd
2	Core 1	Section: D	-0.42	-17.07	50
2	Core 2	Section: A	0.45	-15.05	39
2	Core 2	Section: B	-0.35	-16.78	48
2	Core 2	Section: C	-0.43	-17.69	54
2	Core 2	Section: D	-0.98	-18.38	58
4	Exterior Lamination	4A1	-0.80	-13.07	28
4	Exterior Lamination	4A2	-0.70	-15.52	41
4	Exterior Lamination	4A3	-0.78	-14.00	33
4	Exterior Lamination	4A4	-0.99	-18.82	61
4	Microterracettes	4B1	-0.54	-18.15	57
4	Microterracettes	4B2	-0.79	-19.08	62
4	Microterracettes	4B3	-0.71	-19.07	62
4	Exposed Layer	4C1	nd	nd	nd
4	Exposed Layer	4C2	-0.78	-17.47	52
4	Exposed Layer	4C3	-0.84	-19.04	62
4	Exposed Layer	4C4	-1.21	-20.58	72
4	Exposed Layer	4C5	-0.77	-18.74	60

* Calculations described in the stable isotope section of materials and methods.
nd=no data
All paleotemperature data ±10°C.

Appendix H: Carbon and nitrogen isotope values for acid extracted samples.

Section	Sample Location	ID	Ampl. 28[t] (V)	$\delta^{15}N$ (‰)	% N (%)	Ampl. 44[t] (V)	$\delta^{13}C$ (‰)	% C (%)	C:N*
1	Vent	lily pads (#2)	1.1	-5.6	1.31	2.0	-29.6	7.11	5.44
1	Proximal Slope	sub-green terracettes (#5)	0.7	-2.4	0.82	1.4	-28.3	4.88	5.93
1	Proximal Slope	dry terracettes (#7)	1.2	-2.6	1.72	2.2	-28.6	8.97	5.21
1	Proximal Slope	sub-dry terracettes (#8)	0.4	2.1	0.18	1.7	-27.2	1.56	nd
1	Proximal Slope	leathery mat (#9)	1.5	-1.6	2.46	3.8	-26.3	18.31	7.44
1	Proximal Slope	sub-leathery mat (#10)	1.8	-0.7	2.23	4.5	-26.8	17.62	7.91
2	Handsample	2A	1.4	4.1	0.13	1.8	-23.7	0.70	5.20
2	Handsample	2B	1.3	5.0	0.17	3.5	-22.3	1.02	5.91
2	Handsample	2B[2]	1.2	4.5	0.12	3.7	-22.7	0.78	6.34
2	Handsample	2B[3]	1.2	4.3	0.22	1.5	-21.7	1.06	4.92
2	Handsample	2C	1.2	-0.4	0.16	1.7	-22.9	0.93	5.70
2	Handsample	2D	0.9	3.6	0.10	2.4	-23.2	0.63	6.24
2	Handsample	2E	0.5	5.8	0.07	2.0	-26.7	0.67	9.01
2	Handsample	2E[2]	0.5	6.0	0.05	1.1	-24.2	0.33	6.95
2	Handsample	2E[3]	0.6	3.5	0.06	0.8	-24.0	0.32	5.33
2	Handsample	2F	0.8	3.5	0.08	1.9	-24.6	0.61	7.24
2	Handsample	2F[2]	0.6	-1.1	0.09	0.9	-24.6	0.57	6.18
2	Core 1	Section A	0.9	1.1	0.16	1.9	-26.2	0.78	5.05
2	Core 1	Section B	0.2	2.8	0.06	0.6	-26.0	0.57	nd
2	Core 1	Section C	0.4	-0.1	0.06	1.2	-26.3	0.44	nd
2	Core 1	Section D	0.4	-2.6	0.05	0.8	-26.1	0.35	nd
2	Core 2	Section A	0.4	1.5	0.06	1.1	-26.0	0.37	nd
2	Core 2	Section B	0.3	1.3	0.12	0.9	-25.8	0.92	nd
2	Core 2	Section C	0.4	0.6	0.08	1.2	-25.9	0.55	nd
2	Core 2	Section D	0.4	1.6	0.10	1.1	-26.0	0.60	nd
4	Exterior Lamination	4A1	0.7	3.9	0.09	2.0	-20.1	0.61	7.06
4	Exterior Lamination	4A1[2]	0.2	3.0	0.07	0.5	-20.5	0.66	nd
4	Exterior Lamination	4A2	3.2	0.7	0.17	4.8	-25.9	1.11	6.38
4	Exterior Lamination	4A3	0.5	3.9	0.19	1.2	-24.9	1.28	6.83
4	Exterior Lamination	4A4	1.7	6.0	0.45	5.5	-23.8	3.27	7.26
4	Exterior Lamination	4A4[2]	0.6	6.5	0.19	1.2	-23.4	1.27	6.66
4	Exterior Lamination	4A4[3]	0.9	4.4	0.42	1.1	-24.4	2.20	5.28
4	Microterracettes	4B1	1.7	5.4	0.35	2.5	-24.7	2.16	6.08
4	Microterracettes	4B2	1.5	0.5	0.23	3.9	-26.0	1.29	5.70
4	Microterracettes	4B3	0.6	12.3	0.09	1.8	-24.8	0.59	6.26
4	Exposed Layers	4C1	0.6	1.9	0.17	1.8	-26.7	1.16	6.81
4	Exposed Layers	4C1[2]	0.4	-0.1	0.19	0.6	-25.9	1.30	nd
4	Exposed Layers	4C2	0.6	0.0	0.19	2.0	-27.7	1.32	7.08
4	Exposed Layers	4C3	0.2	3.1	0.11	1.0	-26.2	1.12	nd
4	Exposed Layers	4C3[2]	0.4	3.8	0.08	1.0	-26.2	0.55	nd
4	Exposed Layers	4C5	0.4	2.3	0.06	2.0	-26.6	0.66	nd
4	Exposed Layers	4C5[2]	0.5	0.4	0.13	1.4	-25.0	0.91	6.77
4	Exposed Layers	4C5[3]	0.2	-2.1	0.06	0.5	-26.6	0.57	nd

[t] amplitude 28 related to % N and amplitude of 44 related to % C.

*C:N ratios with N amplitude below 0.5 V were rejected.

nd = no data

[n] indicates replicate number